Rear Inflow in Squall Lines with Trailing Stratiform Precipitation

BRADLEY F. SMULL

Weather Research Program, NOAA Environmental Research Laboratories, Boulder, CO 80303

ROBERT A. HOUZE, JR.

Department of Atmospheric Sciences, University of Washington, Seattle, WA 98195

(Manuscript received 17 July 1986, in final form 7 April 1987)

ABSTRACT

The relative airflow and accompanying precipitation structure of squall lines trailed by mesoscale regions of stratiform rain are examined with emphasis on the occurrence of "rear inflow," i.e. the intrusion of environmental air into these storms across the trailing precipitation boundary. Three cases from Kansas and Oklahoma provide examples of "Strong Rear Inflow," which crosses the back edge of the stratiform precipitation area at relative speeds exceeding 10 m s^{-1}. The vertical profiles of relative flow at the trailing precipitation boundary of these three systems were remarkably similar, with the rear inflow confined to a jet-like layer centered at about 550 mb. Doppler radar data for two of these cases showed that the rear inflow jet occupied a continuous channel extending from middle levels at the back edge of the stratiform region to lower levels of the leading convective region, where it merged with outflow from convective downdrafts to bolster the leading gust front. Strong front-to-rear flow occurred both above and below this layer. The front-to-rear flow lying above the rear inflow jet was consistently strengthened in the vicinity of convective cells and was separated from the rear inflow by an interface of strong vertical wind shear that sloped upward toward the rear of the storm. Soundings indicate this interface marked the division between cloudy air (the trailing "anvil") associated mesoscale updraft (above) and subsaturated air in the mesoscale downdraft (below).

An inclusive review of the literature reveals that these three midlatitude squall lines had stronger rear inflow than any previously described squall lines with trailing stratiform precipitation. Five "Weak Rear Inflow" cases had peak inflows at the back edge of the stratiform rain area between 5 and 10 m s^{-1}. The vertical profiles of relative flow at the trailing edge exhibited a variety of structures, with the rear inflow maximum sometimes at higher altitude and sometimes at lower altitude than in the Strong Rear Inflow cases. The literature further reveals ten studies in which the relative flow at the back edge of the precipitation showed little if any rear inflow (<5 m s^{-1}), suggestive of a stagnation of the midlevel system-relative flow as air at the back edge of the stratiform region moved at or near the speed of the system. These "Stagnation Zone" squall systems, like both the Strong and Weak Rear Inflow cases, exhibited maxima of front-to-rear flow at both upper and lower levels; however, the front-to-rear flow was not as strong as in the Strong Rear Inflow cases. The stagnation layer was located between 650 and 750 mb, considerably below the height of the inflow jet in the Strong Rear Inflow systems. While no appreciable rear inflow occurred at the back edge of Stagnation Zone cases, rear-to-front flow has been observed to develop at midlevels in the interior of their stratiform regions, suggesting that physical processes internal to the mesoscale system are capable of generating rear-to-front flow behind the convective line without the aid of ambient flow entering the storm.

1. Introduction

Rapidly moving squall lines trailed by 50–200 km wide regions of stratiform rain are an important type of organized mesoscale convective system. Tropical cloud clusters and midlatitude mesoscale convective complexes both occasionally exhibit this structure (Houze and Hobbs, 1982). One property of these storms is the tendency for midlevel air at the rear of the stratiform rain area to move at speeds near to or exceeding the speed of the squall line. In the latter case, midlevel air enters the interior of the storm across the rear boundary of the stratiform precipitation region. An example of this "rear inflow" is shown in Fig. 1, which is a conceptual model of a squall-line system that passed over Oklahoma on 22 May 1976. Doppler radar data examined by Smull and Houze (1985) indicated that rear inflow breached the back edge of the trailing stratiform echo at midlevels in this storm. Immediately above lay an opposing current of system-relative flow; this front-to-rear branch of the storm's circulation, which coincided with the mesoscale cloud shield from which the stratiform precipitation fell, was described in detail by Smull and Houze (1987).

In this paper, attention is focused on detailed examination of the rear inflow. The 22 May 1976 squall line is reexamined, and its rear inflow is compared to other cases. The goals are to determine insofar as possible:

1) The magnitude and variability from case to case of airflow across the rear boundaries of squall lines

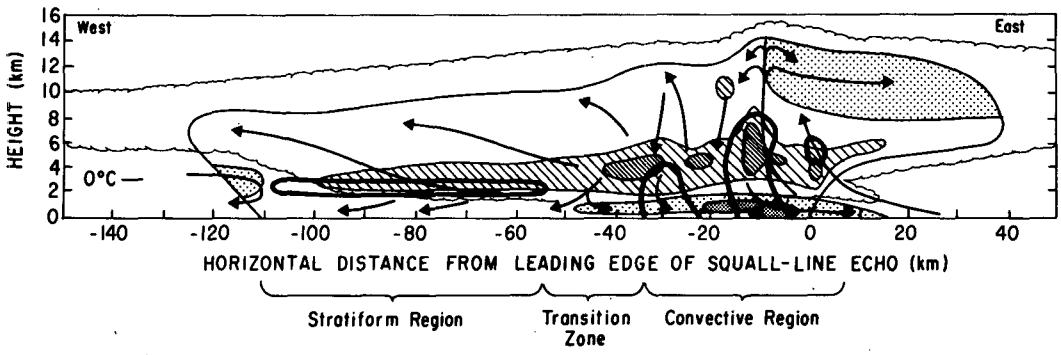

FIG. 1. Conceptual model of the mature 22 May 1976 Oklahoma squall line system viewed in a vertical cross section oriented normal to the convective line. System motion is from left to right (i.e., eastward) at 15 m s^{-1}. Scalloped line marks extent of cloud. Outermost solid contour marks boundary of detectable precipitation echo, while heavy solid lines enclose more intense echo features. Stippling indicates regions of system-relative horizontal wind directed from rear to front (left to right); darker stippling represents stronger flow. Elsewhere within the echo, relative flow is from front to rear (right to left). Maximum front-to-rear flow at middle and upper levels is shown by hatching; darker hatching denotes embedded speed maxima. Thin streamlines show two-dimensional projection of relative flow determined from the dual-Doppler analysis and the composite rawinsonde analysis of Ogura and Liou (1980). The 0°C level in the trailing stratiform region is indicated at rear of the echo. (From Smull and Houze, 1987.)

with trailing mesoscale regions of stratiform precipitation.

2) The spatial and temporal variability of the rear inflow within these storms.

In a pioneering study, Newton (1950) examined a squall line trailed by a 200 km wide region of stratiform rain and deduced qualitatively that rear inflow was present. However, neither its strength nor its temporal or spatial variation within the storm were determined. Since then, profiles of relative airflow have been measured to the rear of many such systems. We have deduced the existence and magnitude of rear inflow in a substantial number of these cases from the figures and tables that were presented in previous studies (Table 1). Rear inflow was not a primary concern of these previous studies, and this aspect of the airflow has never been compared among the various cases.

With some exceptions, which will be noted in later sections, the previous studies cited in Table 1 provide little information on the spatial or temporal variability of rear inflow structure. Further analysis of the 22 May 1976 storm together with data from two squall lines observed in the 1985 Oklahoma-Kansas PRE-STORM[1] field experiment help fill this gap. High-frequency rawinsonde data obtained for the 22 May 1976 squall line allow us to investigate the rear inflow associated with that case in some detail. That analysis, which is described in section 2, suggests that the schematic structure in Fig. 1 represents an early stage of the rear inflow's development. The soundings show that subsequent to the period of Doppler radar observations upon which the horizontal flow in Fig. 1 was based, the rear inflow strengthened and penetrated well into the storm—perhaps so far as to reach its leading gust front. [This evolution was hypothesized by Smull and Houze (1985) on the basis of marked changes in the radar reflectivity pattern.] As shown by Table 1, sounding data for the 22 May 1976 squall line establish its rear inflow to have been stronger than any of those described in previous literature.

The two PRE-STORM cases, which are the last entries in Table 1, are described in section 3. Doppler radar data are used to show that the strong rear inflow observed on 22 May 1976 was not anomalous, but in fact recurred in very similar fashion (as did other notable aspects of storm structure) in these two independent cases. Furthermore, the PRE-STORM data allow the rear inflow to be described in unprecedented detail. They illustrate its extension across the trailing stratiform region and merger with outflow from convective cell downdrafts, where it evidently bolstered the leading gust fronts of both storms.

In section 4 we refer to a Doppler radar analysis performed by Chong et al. (1987). Their results, together with those of Leary and Rappaport (1987), emphasize the importance of processes internal to the precipitation region in promoting the development of rear-to-front flow within a squall system, even in the absence of rear inflow at the back edge of its stratiform rain area.

The case studies described in sections 2–4 and the wind profiles gleaned from the literature (Table 1) are assimilated in section 5 to yield a more complete description of the airflow at the rear of squall lines with trailing stratiform precipitation than has heretofore been attempted. We identify contrasting regimes of relative flow at the rear of squall-line systems. Some

[1] *P*reliminary *R*egional *E*xperiment for *STORM*-Central. STORM is the National *ST*ormscale *O*perational and *R*esearch *M*eteorology Program. See Cunning (1987) for a description of the project.

TABLE 1. Studies reporting relative flow to the rear of squall lines with trailing stratiform precipitation. Under heading "Maximum Strength of Rear Inflow," positive values denote the peak speed of rear inflow (i.e., rear-to-front, system-relative flow); in cases where rear inflow was not observed, negative values represent the weakest outflow (i.e., front-to-rear, system-relative flow) in the vertical profile. "Source of data" refers to the wind profile used to determine the strength and pressure level of maximum rear inflow (although other data types may have been presented in the study).

Study	Location	Type of analysis	Source of data	Maximum strength of rear inflow $(U_n)_{max}$ (m s^{-1})	Pressure level of rear inflow maximum (mb)	Squall line propagation speed (m s^{-1})
Previous Studies:						
Zipser (1969)	Tropical W. Pacific	Case study	Rawinsonde	7	800	15
Obasi (1974)	Tropical W. Africa	Composite (21 cases)	Rawinsonde	2	890	?
Betts et al. (1976)	Venezuela	Composite (4 cases)	Rawinsonde	2	800, 550	14
Houze (1977)	Tropical E. Atlantic	Case study	Rawinsonde	7	720	12
Zipser (1977)	Barbados	Case study	Rawinsonde	−4	800	17
Zipser & Matejka (1982)	Illinois	Case study	Doppler radar	7	580	14
Gamache & Houze (1982)	Tropical E. Atlantic	Case study	Rawinsonde	1	670	14
Fernandez (1982)	Tropical W. Africa	Composite (3 cases)	Rawinsonde	1	500	15
Kessinger et al. (1983)	Oklahoma	Case study	Rawinsonde	2	450	10
Houze & Rappaport (1984)	Tropical E. Atlantic	Case study	Rawinsonde	5	700	7
Drosdowsky (1984)	Northern Australia	Case study	Rawinsonde	1	630	14
Schmidt & Cotton (1985)	Montana	Case study	Doppler radar	7*	450	22
Chong et al. (1987)	Tropical W. Africa	Case study (22 June '81)	Doppler radar	−1	775	19
Leary & Rappaport (1987)	West Texas	Case study	Rawinsonde	3	500	12
Roux (1987)	Tropical W. Africa	Case study (23 June '81)	Doppler radar	4	640	14
This Paper:						
22 May 1976	Oklahoma	Case study	Rawinsonde	17	630	15
28 May 1985	Kansas (PRE-STORM)	Case study	Doppler radar	16	580	17
10 June 1985	Kansas (PRE-STORM)	Case study	Doppler radar	16	560	14

* Later increased to 12 m s^{-1} (Jerome Schmidt, personal communication).

storms (e.g., the 22 May 1976 case and the two PRE-STORM squall lines) develop a strong, jet-like rear inflow (represented by large positive velocities in Table 1), while others are characterized by rather weak inflow (sometimes nearly zero or even slightly negative, the latter denoting weak front-to-rear flow). Air motions in the latter group are more suggestive of a stagnation zone than a jet. From this synthesis, an overview of the rear inflow phenomenon is obtained. It represents the first effort to obtain a comprehensive description of the frequency of occurrence, strength, vertical structure, horizontal variation and evolution of rear inflow in squall lines with trailing stratiform precipitation. To the extent that rear inflow represents a feedback capable of altering the strength and evolution of the parent storms, this study provides quantitative insight into the interaction of mesoscale convective systems with their large-scale environments.

2. Rawinsonde data for the 22 May 1976 squall-line system

a. *Data and method of analysis*

As part of its 1976 Spring Program, the National Severe Storms Laboratory (NSSL) operated a sounding network consisting of nine sites spaced ≈50 km apart across central and western Oklahoma. Their locations and respective three-letter identifiers are shown in Fig. 2. On 22 May 1976, soundings were released at nine nominal times: first at 0900,[2] and then at 90 min intervals from 1300–2330; in all, 80 ascents were recorded. It was during the latter part of this period that the squall line passed through the network. In our analysis, each sounding was located with respect to the leading edge of the low-level radar echo corresponding to the line of intense convective cells in a manner similar to that described by Ogura and Liou (1980), except that deviations of the line's orientation from its mean north–south alignment were taken into account. Profiles of temperature, dewpoint, relative humidity (with respect to liquid water and ice), wet-bulb potential temperature (θ_w) and *system-relative* wind (relative to the squall line, which moved eastward at a mean speed of 15 m s^{-1}) were analyzed for each sounding.

Although the precipitation and kinematic structures of the squall system were two-dimensional in their gross characteristics (Ogura and Liou, 1980; Smull and Houze, 1987), a notable asymmetry developed near

[2] Unless otherwise noted, all times are CST (UTC − 6 h).

the center of the storm's back edge, where the stratiform radar echo eroded to form a notch-like concavity (Smull and Houze, 1985). Subsequently, a downstream segment of the convective line rapidly bowed forward. The present analysis emphasizes those soundings taken within a swath extending from behind the notch toward the bowing segment of the convective line. It was in this zone that the rear inflow was found to be most intense. The soundings presented here span a broad range of locations in the X-direction (measured positive ahead and negative behind the line, as in Fig. 1), and thus illustrate changes in the rear inflow's structure as a function of distance from the squall line. In several instances, soundings obtained at similar system-relative locations but at different times provide some indication of flow evolution. The location of each sounding vis-a-vis the low-level radar echo pattern at the time of the balloon's launch is illustrated in the inset portion of Figs. 3–8 to aid interpretation of the data. Reflectivity patterns are from NSSL's WSR-57 S-band radar, which was co-located with the OUN sounding site shown in Fig. 2.

b. *Advance of rear inflow across the trailing stratiform region*

Westerly winds so strong as to overtake the system extended far behind the leading "nose" of rear inflow shown entering the stratiform region near $X = -115$ km in Fig. 1. The LTS 2331 sounding (Fig. 3) released at $X = -255$ km, farther behind the storm than any other, encountered rear inflow in the layer from 640

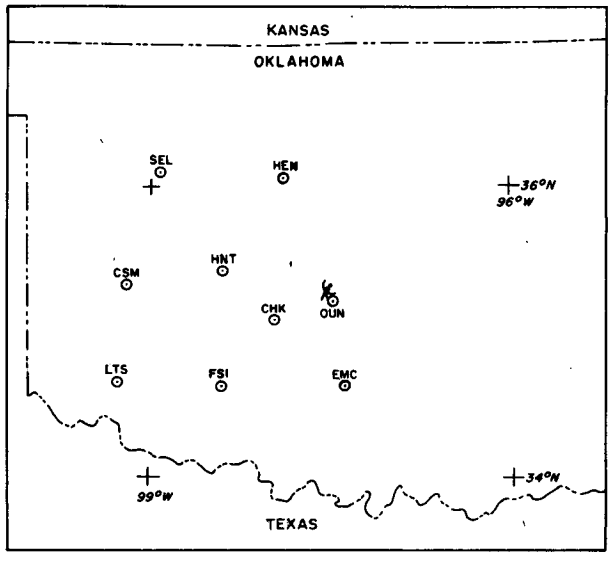

FIG. 2. Location of special rawinsonde sites (with their respective three-letter identifiers) operated during the 1976 NSSL Spring Program. Also shown is NSSL's WSR-57 S-band conventional radar, located at OUN.

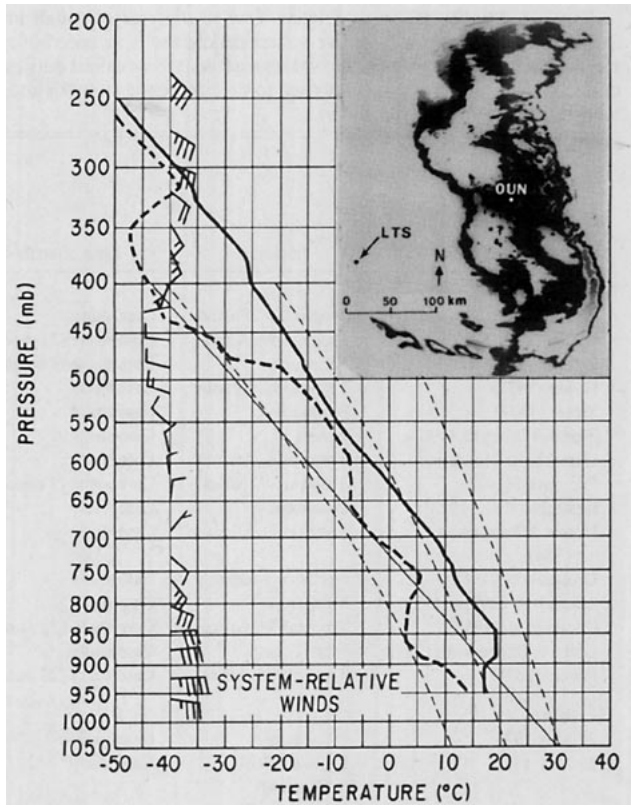

FIG. 3. Sounding taken at 2331 CST 22 May 1976 at LTS, located at $X = -255$ km (see text for explanation of coordinates). Light solid and dashed lines are dry and moist adiabats, respectively. Temperature and dewpoint are indicated by heavy solid and dashed lines, respectively. Also shown is the *system-relative* wind profile determined by subtracting a mean squall line motion of 270° at 15 m s^{-1} from the observed (ground-relative) winds. Wind plotting convention: pennant, 12.5 m s^{-1}; full barb, 5 m s^{-1}; half barb, 2.5 m s^{-1}. Inset at upper right shows the location of the rawinsonde site relative to the horizontal reflectivity pattern at the time of release. Reflectivity levels (dimly visible) measured by NSSL's WSR-57 radar are: minimum detectable, 21, 31, 42 and 52 dBZ. Horizontal scale and north direction are indicated.

to 380 mb (3.4 to 7.4 km)[3]. The strongest inflow corresponded to west-northwest relative winds at 520 mb in Fig. 3. Winds backed sharply with height in the layer immediately below the trailing cloud base at 310 mb. Within the cloud layer strong southeasterly relative winds and ice-saturated conditions marked a continuation of the mesoscale front-to-rear airflow described by Smull and Houze (1985, 1987) and shown in Fig. 1. Moist conditions in the 600–500 mb layer were atypical of soundings behind the storm, and probably resulted from convection developing along the southern edge of its wake (bottom of inset in Fig. 3).

[3] For consistency with the radar-based coordinates used by Smull and Houze (1987), all reported heights are above ground level as measured from NSSL's primary Doppler radar site at Norman (OUN), located at 361 m above mean sea level.

The HNT 2330 sounding (Fig. 4), released at $X = -130$ km, locates the strongest rear inflow between 500 and 600 mb, just below the trailing stratiform cloud. Over the intervening 125 km between the soundings shown in Figs. 3 and 4, the core of strongest rear inflow dropped from 500 to 590 mb (5.4 to 4.1 km) and strengthened, with an increase of about 5 m s^{-1} in the U-component.

Evolution of the rear inflow is suggested by two soundings taken about one hour apart near the heart of the trailing stratiform echo (CSM 2055 and FSI 2206, shown in Figs. 5 and 6, respectively). Both soundings were located approximately 85 km behind the convective line, although the later one was released 75 km farther south, nearer to the center of the rear echo notch. At the earlier time (Fig. 5), the trailing stratiform cloud base was located near the sounding's termination at 720 mb (2.5 km), and front-to-rear (northeasterly) relative winds filled the entire subcloud layer. One hour later at FSI (Fig. 6), subsaturated and potentially cool rear inflow air dominated the layer from 850 mb (1.1 km) through the top of the sounding at 575 mb (4.3 km). The 17 m s^{-1} relative wind at 680 mb (2.9 km) was the largest rear inflow speed measured near the back edge of the stratiform region, and was thus entered in Table 1. By contrast, the maximum inflow speed measured by Doppler radar in the north part of the notch some 30 min earlier was 12 m s^{-1}. A significant decrease of relative humidity accompanied the stronger rear inflow; a cloud base near 720 mb (2.5 km) was indicated at CSM, whereas unsaturated conditions existed up through 575 mb (4.3 km) at FSI. These changes are consistent with pronounced evaporation of cloud and precipitation into the rear inflow air.

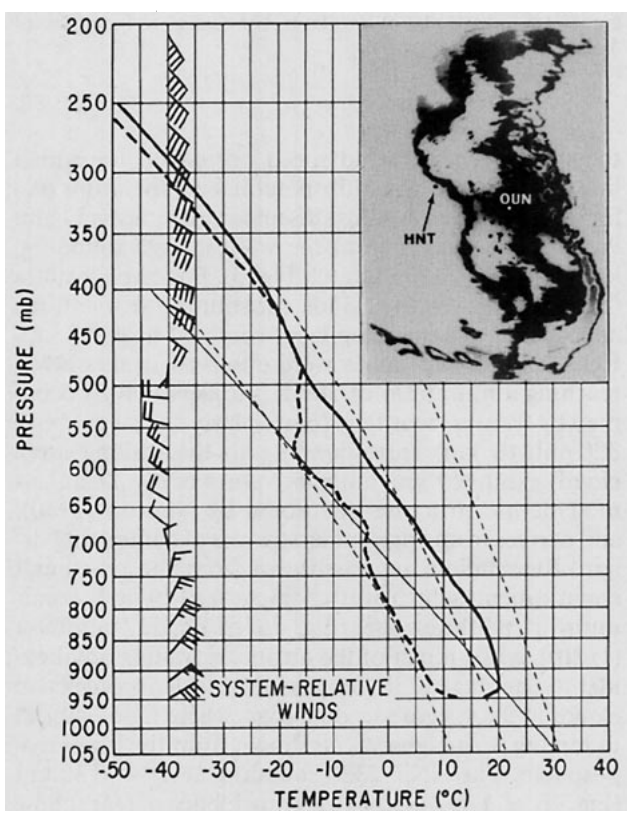

FIG. 4. As in Fig. 3 except for 2330 CST at HNT, located at $X = -150$ km.

The interpretation of differences between Figs. 5 and 6 is complicated by the fact that the soundings were taken at different north–south locations relative to the notch. The radar echo history, which showed erosion of stratiform echo in the notch region and marked forward acceleration ("bowing") of an adjacent segment of the convective line (cf. insets of Figs. 5 and 6; also, Fig. 4 of Smull and Houze, 1985), suggests that rear inflow penetrated well into the storm and ultimately reached the convective line. However, since in comparing Figs. 5 and 6 it is impossible to separate the effects of evolution from those of flow variation in the along-line direction, this hypothesized evolution remains somewhat speculative.

Most soundings released into precipitation between $X = -85$ km and the front of the storm were truncated even more severely than those shown in Figs. 5 and 6, probably as balloons were lost due to extreme vertical wind shear or icing. However, important changes of the relative flow structure are evident in two soundings taken $\approx$3 h apart just ahead of the convective line. Figure 7 shows the 1900 LTS sounding, released near an intense convective cell as the squall line entered the NSSL network. [The apparent collocation of the sounding with an intense echo seen in the inset is misleading, since at the time of release the observer reported the leading edge of precipitation to be about 10 km to the west-northwest. The intense echo was likely return from a new cell located aloft which intersected the top of the beam near the 4.5 km level.] The thermodynamic profile is typical of that in convective updrafts (Davies-Jones, 1974); with the exception of the layer from 545 to 500 mb (immediately above the 0°C level), where thermistor icing evidently influenced the thermodynamic measurements, the lapse rate above the lifting condensation level (775 mb, 1.9 km) was moist adiabatic. The wind profile indicates that air below 540 mb (4.8 km) was overtaken by the system, while air was entering the leading anvil above that level. Gust front passage occurred about 10 min after the sonde was released, and hence is not evident in the profile. The 2200 EMC sounding (Fig. 8)[4] was taken near the echo's leading edge at the northern end of the bowing segment of the convective line, which lay in

[4] The suspect thermodynamic structure at middle levels in Fig. 8 (i.e., the superadiabatic lapse rate accompanied by rapid drying immediately above the 620 mb level) likely resulted as the rawinsonde emerged from a sloping convective updraft core and came into contact with unsaturated air. In this process, the wet thermistor would briefly cool to the wet-bulb temperature.

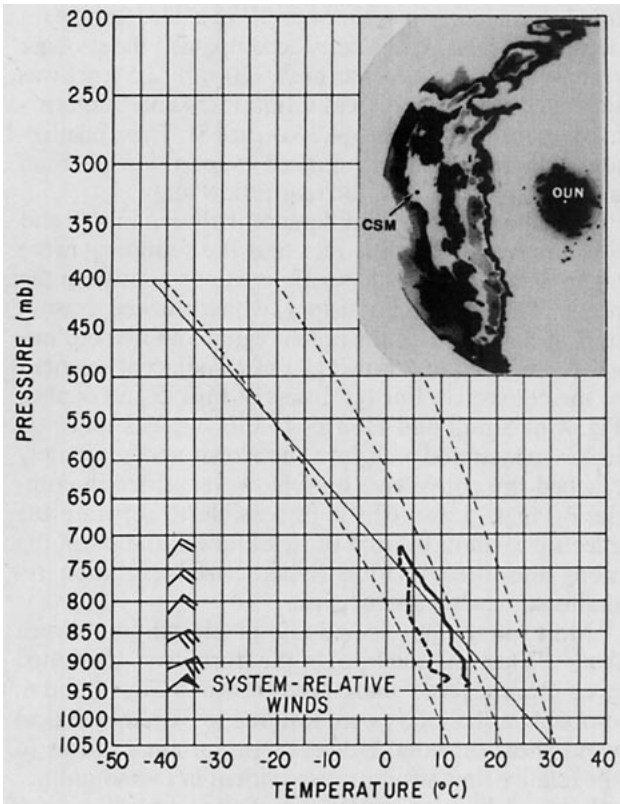

FIG. 5. As in Fig. 3 except for 2055 CST at CSM, located at $X = -85$ km.

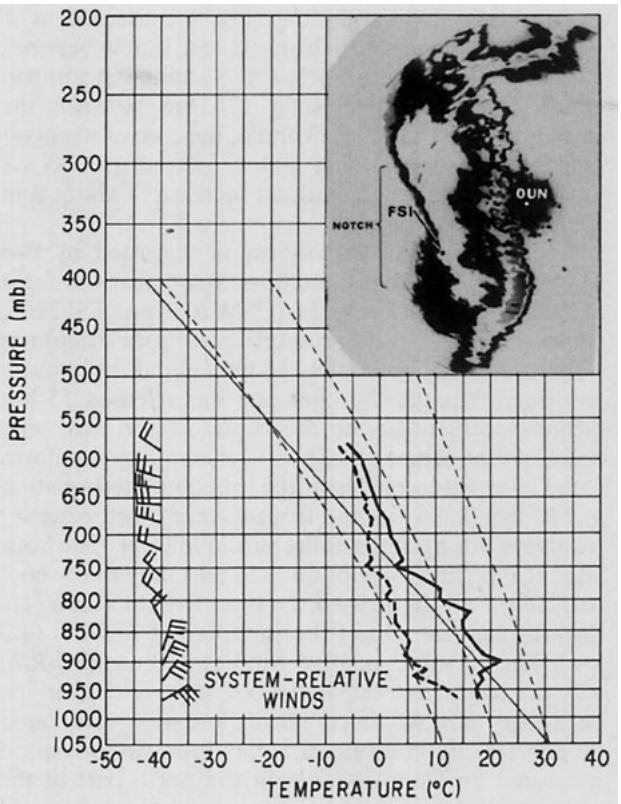

FIG. 6. As in Fig. 3 except for 2206 CST at FSI, located at $X = -85$ km. Notch in back edge of stratiform echo (described in text) is indicated in the inset.

the projected path of the strongest rear inflow found near the rear echo notch. The presence of cool air in the surface—875 mb layer moving at or faster than the speed of the system—indicates that the gust front had already passed. An important difference between Figs. 7 and 8 is the apparent development of the mid-level maximum of front-to-rear relative flow during the 1900–2200 interval. This mesoscale feature, shown by hatching in Fig. 1, appeared prominently in the 2040 and 2135 Doppler velocity analyses of Smull and Houze (1985, 1987). While the earlier sounding exhibited an increasing westerly component with height up to 350 mb (8.5 km), Fig. 8 reveals a more complex wind profile. Stronger front-to-rear relative flow (marked by an appreciable easterly wind component) had developed, with air entering the front of the storm in a deep layer centered near 575 mb (4.3 km). Since the dual-Doppler analysis showed that front-to-rear flow strength varied little on the mesoscale in the along-line direction, we conclude that these soundings document the development of mesoscale rearward flow at middle levels. This remarkable kinematic change coincided with a period in which the overall width of the trailing stratiform echo was increasing.

To describe further the path of rear inflow air across the stratiform region, Fig. 9 presents paired profiles of the system-relative wind speed normal to the squall line (U) and the wet-bulb potential temperature (θ_w) for several of the soundings discussed previously. Figure 9a contains profiles from the westernmost sounding, located at $X = -255$ km (cf. Fig. 3). Positive U values (i.e., westerly relative winds constituting rear inflow) appear in a $\approx$3 km deep layer centered near 5.5 km. Relatively low θ_w values were observed in this layer, reaching a minimum of 289 K. Adjacent levels occupied by front-to-rear flow [particularly the layer above 320 mb (8 km) corresponding to the trailing anvil cloud] exhibited much higher values of θ_w. This thermodynamic structure was noted by Newton (1950), and derives from adjacent airstreams of contrasting origin. Rear inflow air was drawn from the postsquall environment, which was characterized by a θ_w minimum at midlevels [see Fig. 19 of Ogura and Liou (1980)], while much of the air in the trailing anvil evidently originated in or passed between convective clouds at the system's leading edge, where it was subject to mixing with higher θ_w air drawn from the lower troposphere. The HNT 2330 sounding at $X = -130$ km (Fig. 9b, cf. Fig. 4) shows the coincidence of rear inflow (centered near 4 km) with a minimum θ_w of $\approx$289 K. This persistent association of the strongest rear inflow

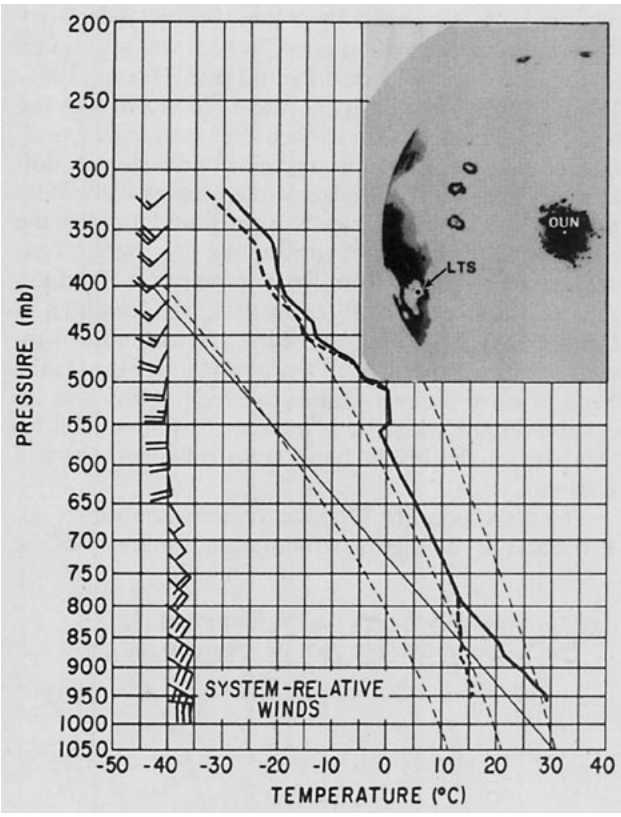

FIG. 7. As in Fig. 3 except for 1900 CST at LTS, located at $X = +10$ km.

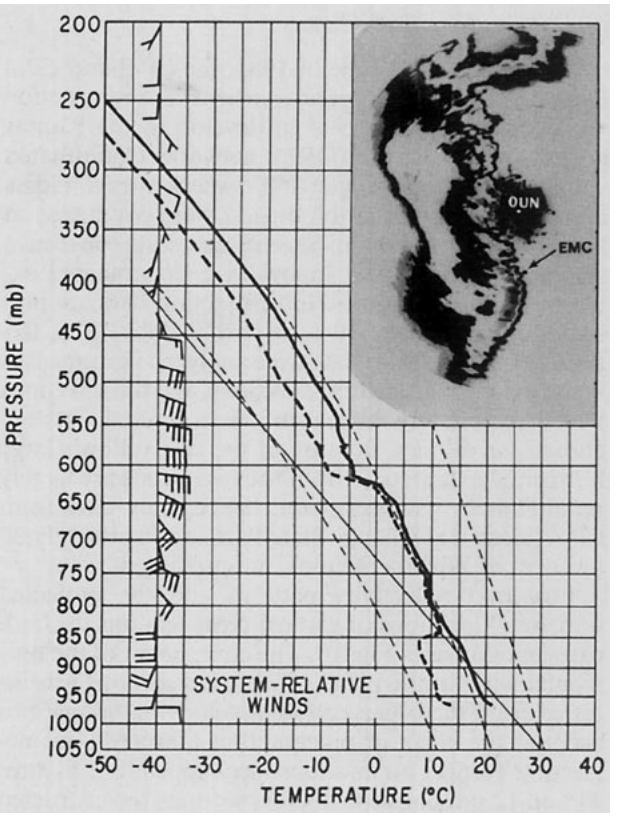

FIG. 8. As in Fig. 3 except for 2200 CST at EMC, located at $X = +5$ km.

with low θ_w values indicates that rear inflow air was descending as it traversed the storm. This inference is also supported by the findings of Ogura and Liou (1980), who diagnosed a mesoscale downdraft in the lower troposphere in the trailing stratiform region.

The axis of strongest rear inflow sloped downward through the 0°C level, where the melting of stratiform precipitation produced a sharp increase of radar reflectivity (note the bright-band echo indicated in the interval $-100 < X < -50$ km in Fig. 1). The influence of melting is seen in the 2206 FSI θ_w profile, measured well within the stratiform precipitation region (Fig. 9c, cf. Fig. 6). Once again, depressed θ_w values mark the rear inflow layer between 1 and 4 km, straddling the melting level near 3 km. Values just above and well below the melting layer remained close to the upstream value of 289 K. However, air that had recently been in contact with melting precipitation (as implied by its location at and immediately below the 0°C level) exhibited θ_w values as low as 286 K, representing 3 K of diabatic cooling. If this cooling is assumed to have occurred over the period required for parcels to traverse the distance between the sounding site and the radar echo's back edge, a cooling rate may be determined. Taking a typical relative windspeed (15 m s^{-1}) and the length of trajectory in precipitation ($\approx$40 km), the corresponding rate of cooling is $\approx$4 K h^{-1}. This value agrees well with the results of Leary and Houze (1979), who estimated cooling rates of 1–7 K h^{-1} in the melting layers of tropical squall line systems exhibiting structure similar to the Oklahoma storm. Figure 9c also suggests that rear inflow penetrated into the stratiform region well beyond the point shown by Doppler radar 30 min earlier.

3. Rear inflow structure observed in the 1985 Oklahoma-Kansas PRE-STORM experiment

Although observations of strong, downward-sloping rear inflow in the 22 May 1976 storm suggest that it ultimately extended to the squall line's leading edge, the available data were inadequate to make this determination conclusively. Measurements obtained in two very similar storms, which occurred during the PRE-STORM experiment, fill this observational gap. These more recent data allow us to trace the rear inflow forward to the leading convective lines of these storms and thus establish the significance of rear inflow as a mesoscale feedback capable of influencing the parent squall-line convection.

a. Data and method of analysis

During May and June of 1985, the CP-3 and CP-4 Doppler radars[5] were operated whenever precipitation was occurring or expected to develop in the Kansas portion of the PRE-STORM network. Coordinated volume scans, consisting of 360° sweeps by both radars at a sequence of elevation angles, were conducted at least three times per hour. Several mesoscale convective systems exhibiting rear inflow were documented extensively in this manner. In this section data are presented for two cases: 10 June and 28 May 1985. Reflectivity and velocity data were analyzed in numerous vertical (range–height) cross sections, and those sections which best capture the rear inflow structure have been chosen for display. Because of the rear inflow's large horizontal extent, data from the two radars are largely redundant in its description; hence, only data from CP-4 (located at Cheney State Park, approximately 30 km west of Wichita, Kansas) are presented.

Low-level reflectivity patterns and the projected horizontal locations of vertical cross sections for both cases are shown in Fig. 10. The component of the horizontal wind in the plane of the cross sections was inferred from the observed radial velocities, taking into account the effect of precipitation fallspeeds but neglecting vertical air motions (see Appendix). Figures 11 and 12 present vertical cross sections reconstructed from the volume scans conducted over the intervals 2145–2153 10 June and 0701–0713 28 May, respectively. By convention, airflow away from the radar is represented by positive values, while that toward the radar is negative; arrows indicating flow direction are included for clarity. Heights are above ground level as measured from the CP-4 radar site, located at 438 m MSL. Both systems exhibited intense convective precipitation cores organized along squall lines trailed by lighter stratiform precipitation (Fig. 10).

b. Vertical cross sections

Figure 11 depicts reflectivity and velocity patterns for two cross sections separated by 180° in azimuth through the 10 June 1985 squall line. When joined along their 0 km edges, these sections constitute the continuous vertical plane oriented normal to the squall line whose projection is shown in Fig. 10a. Together they elucidate key features of the precipitation and flow patterns. As viewed in Fig. 11, the system moved from left to right at about 14 m s^{-1}.

The reflectivity pattern (Figs. 11a and 11c) shows the leading line of convective cells (in the 55–95 km range interval) ahead of an extensive region of stratiform precipitation marked by a bright band (from −65 to +40 km range) at the melting level. These contrasting regimes were separated by a low-altitude reflectivity minimum, or "transition zone," which was also noted in the 22 May 1976 case (Smull and Houze, 1985, 1987). Another similarity to the 1976 storm was the tendency for convection to occur in an organized multicellular mode; new cells apparently developed aloft at the system's leading edge, while progressively older mature and dissipating cells were found toward the rear. While the region of continuous precipitation extended over 150 km from front to rear at the surface, the detectable echo aloft (comprising the leading and trailing anvil structures) exceeded 250 km in front-to-rear extent. At the time of the analysis in Fig. 11, the band of most intense stratiform precipitation was located over the radar; it is indicated by increased reflectivity of the bright band echo between −20 and +20 km.

The corresponding Doppler velocity analyses (Figs. 11b and 11d) define the structure and intensity of the

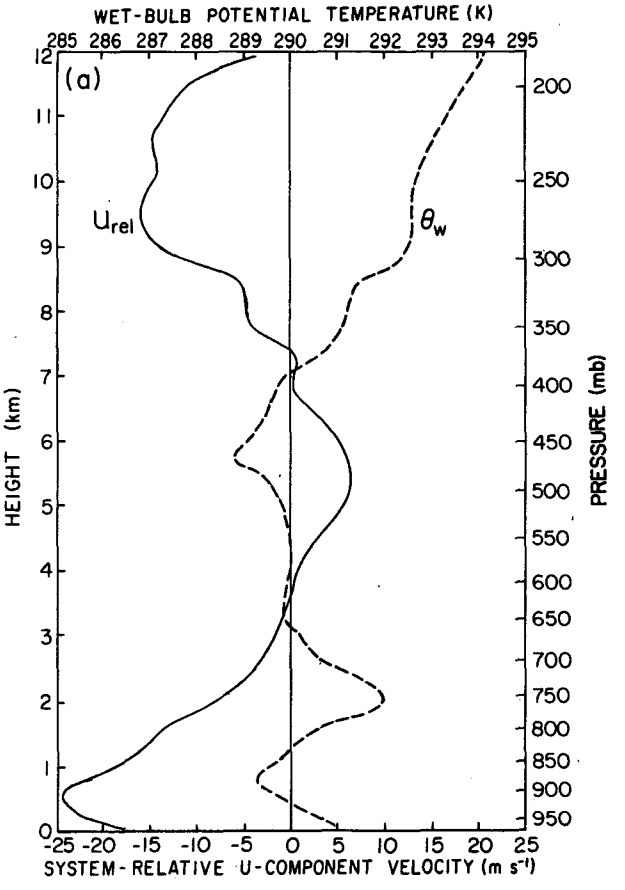

FIG. 9. (a) Profiles of system-relative U-component wind speed (m s^{-1}, solid curve) and wet-bulb potential temperature θ_w (K, dashed curve) derived from 2331 CST sounding at LTS, located at $X = -255$ km (see Fig. 3). Heights are above ground level as measured at Norman, Oklahoma (OUN), located at 361 m MSL. (b) As in panel (a), except for 2330 CST at HNT, located at $X = -150$ km (see Fig. 4). (c) As in panel (a), except for 2206 CST at FSI, located at $X = -85$ km (see Fig. 6).

[5] These 5 cm (C-band) radars, operated by the National Center for Atmospheric Research, were located on a 60 km baseline in southcentral Kansas.

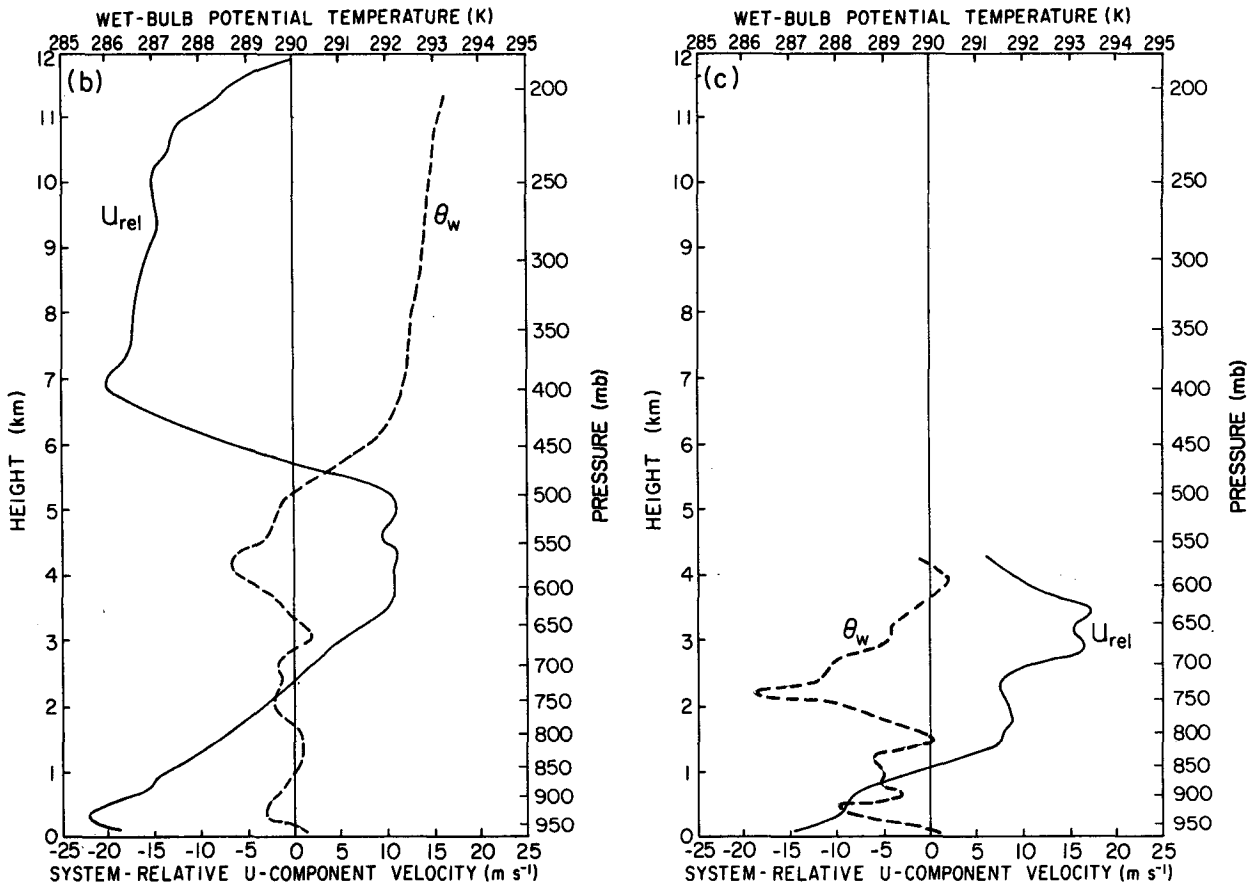

FIG. 9. (*Continued*)

rear inflow in much greater detail than possible with rawinsonde data. The axis of strongest flow approached the system from the rear (directed from left to right in Fig. 11) and sloped downward, paralleling the zone of closely spaced reflectivity contours at the base of the trailing stratiform echo. This juxtaposition indicates that the rear inflow was associated with substantial evaporation of precipitation falling into it. From there, the maximum flow extended forward and downward through the layer of melting stratiform precipitation (marked by the bright band). Similar flow structure was evident in a time–height analysis of data collected over a period of several hours in the stratiform region of this storm by a 50 MHz wind profiler located at McPherson, Kansas, approximately 65 km north-northeast of the CP-4 radar (Augustine and Zipser, 1987).

Figure 11d shows the extension of rear inflow into the convective region. After crossing the transition zone, the mesoscale rear inflow current apparently merged with outflow from convective downdrafts spreading beneath intense cells (e.g., the pocket of velocities in excess of 10 m s^{-1} at 75 km). The resulting mixture of air continued forward to the leading gust front, which is not visible in Fig. 11 due to the elevated height of the beam at extreme range. However, the Doppler radar data convincingly illustrate that rear inflow penetrated sufficiently forward to have been able to influence the intensity and propagation of the deep convection at the system's leading edge.

Immediately above the rear inflow lay an opposing branch of front-to-rear relative flow analogous to that found in the 22 May 1976 squall system (Smull and Houze, 1985, 1987). This current originated ahead of the squall line (as shown by relative speeds < -20 m s^{-1} at the 6 km level near 95 km in Fig. 11d), but deepened and strengthened as it passed through the zone of strong convection. Local speed maxima (identified by closed -30 m s^{-1} contours near 74 and 88 km range) developed near convective reflectivity cores. As in the 1976 case, these speed maxima frequently appeared immediately upstream (ahead) of convective cells at middle levels. Laden with precipitation and cloud-ice particles detrained from the deep convection, this air continued rearward and upward into the trailing stratiform region. The rear inflow and front-to-rear flow met along an interface marked by very intense vertical shear, of order 10^{-2} s^{-1}. This mesoscale shear zone

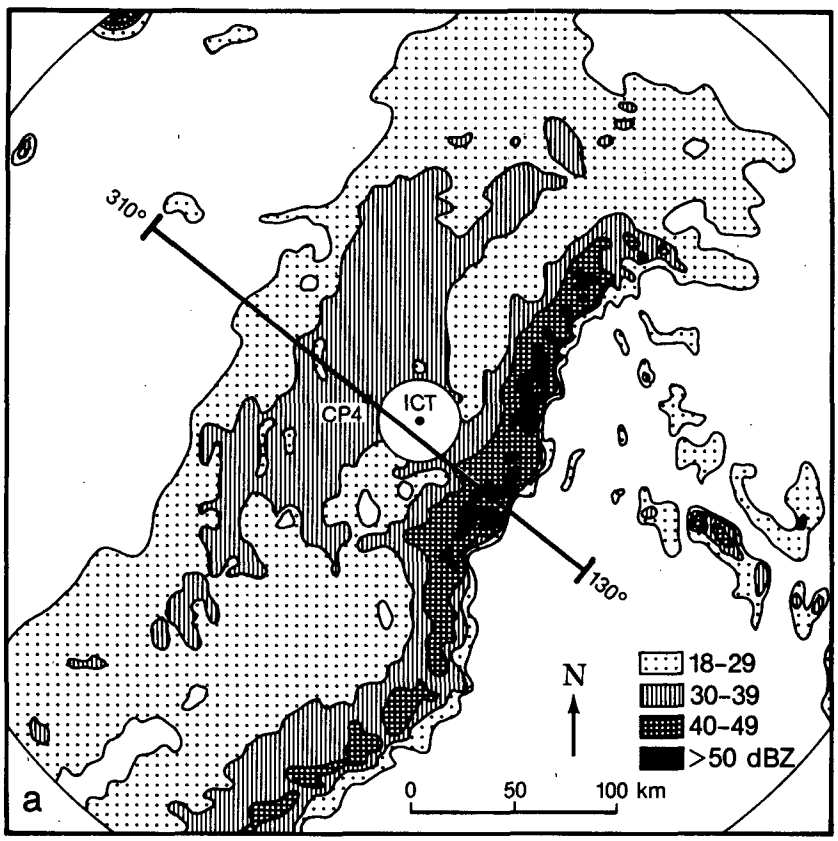
310°
CP4
ICT
130°
N
18-29
30-39
40-49
>50 dBZ
0
50
100 km
a

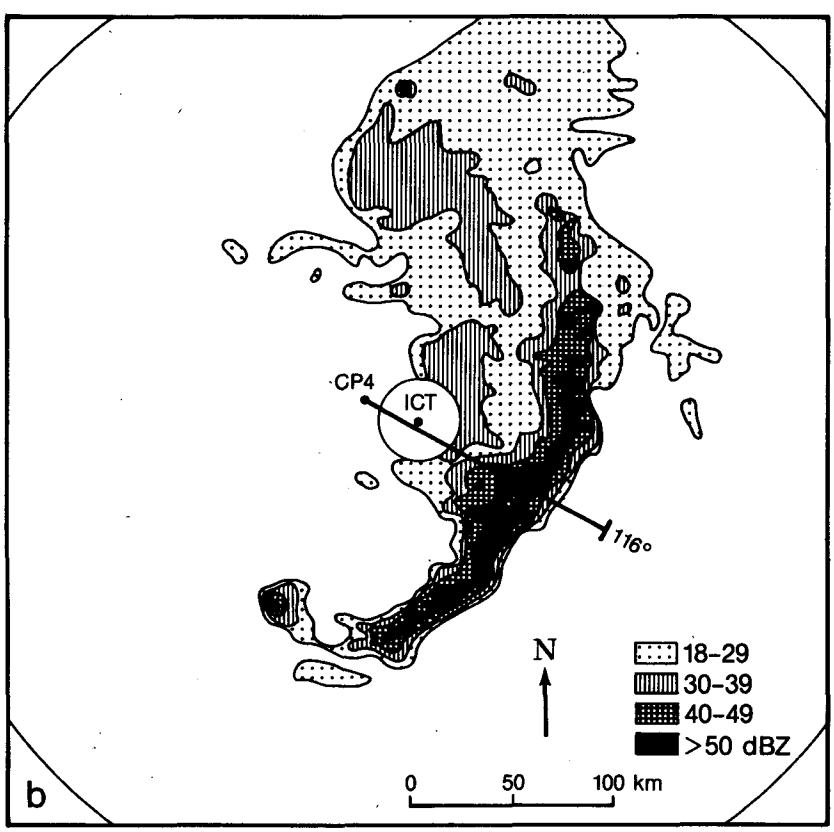
CP4
ICT
116°
N
18-29
30-39
40-49
>50 dBZ
0
50
100 km
b

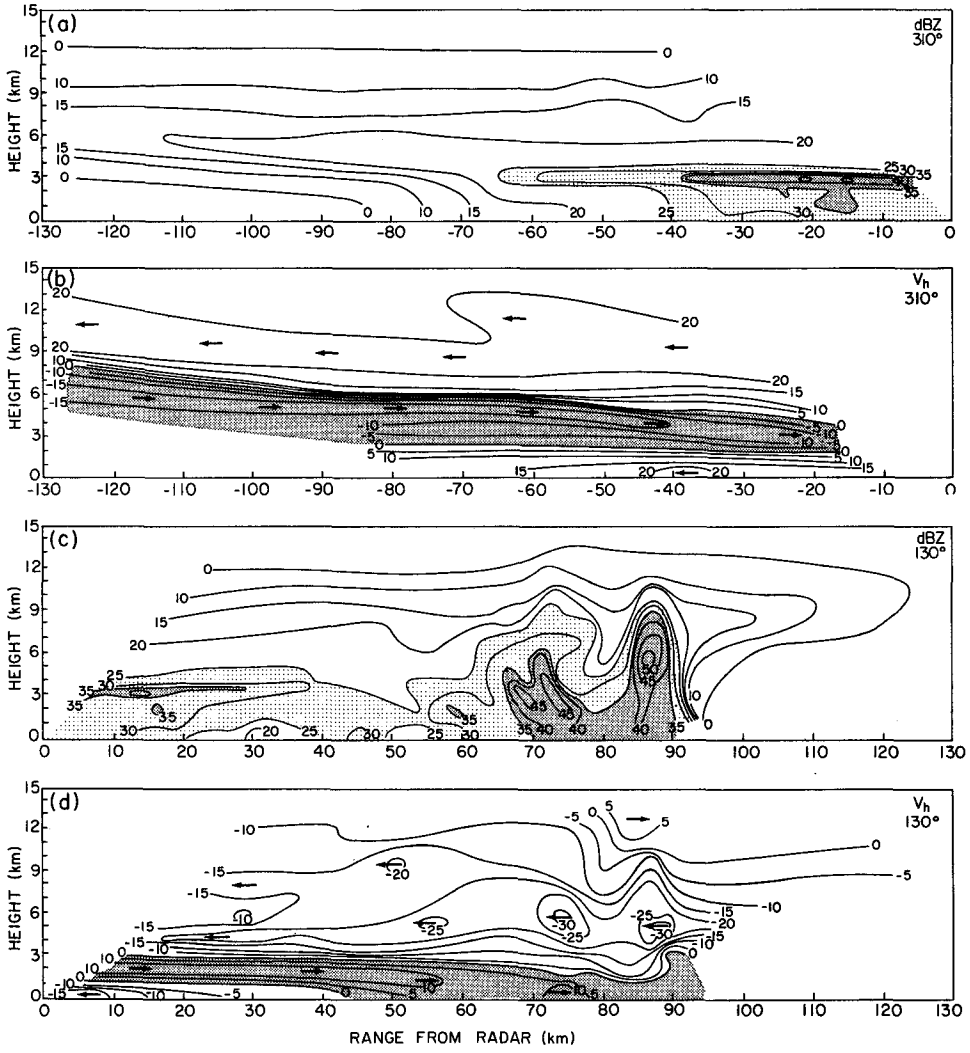

FIG. 11. Vertical cross sections constructed from volume scan conducted from 2145 to 2153 CST 10 June 1985 by the CP-4 C-band Doppler radar. Panels (a) and (b) depict reflectivity (dBZ) and system-relative horizontal velocity (m s^{-1}), respectively, along the 310° azimuth direction; (c) and (d) are analogous displays along 130° azimuth. Height above ground level (km) and range from the radar (km) are indicated. Positive velocities represent flow away from radar while negative velocities denote flow toward radar; arrows indicating flow direction are also shown. Rear inflow (described in text) is highlighted by shading in (b) and (d).

sloped upward toward the rear of the system, signifying convergence of the line-normal flow component at midlevels in the stratiform region. A second sloping interface (again marked by a zero velocity contour and strong shear, but in a sense indicating divergence of the line-normal flow) separated the rear inflow from a layer of rearward flow exiting the stratiform region at low levels. A similar three-tiered arrangement of sloping flows within the trailing anvil region of another mid-latitude (Illinois) squall line has been documented by Srivastava et al. (1986). Moreover, this particular vertical arrangement of line-normal convergence and di-

FIG. 10. Low-level (0.7° elevation) reflectivity structure from Wichita, Kansas (ICT) WSR-57 S-band radar with superimposed locations of vertical cross sections extending from CP-4 C-band Doppler radar located at Cheney State Park (approximately 30 km west-northwest of the Wichita radar). Ground clutter region within 20 km of ICT has been blanked out. Horizontal scale and north direction are indicated. (a) Reflectivity pattern for 2140 CST 10 June 1985 showing location of cross sections shown in Fig. 11. (b) Reflectivity pattern for 0701 CST 28 May 1985 showing location of cross section shown in Fig. 12.

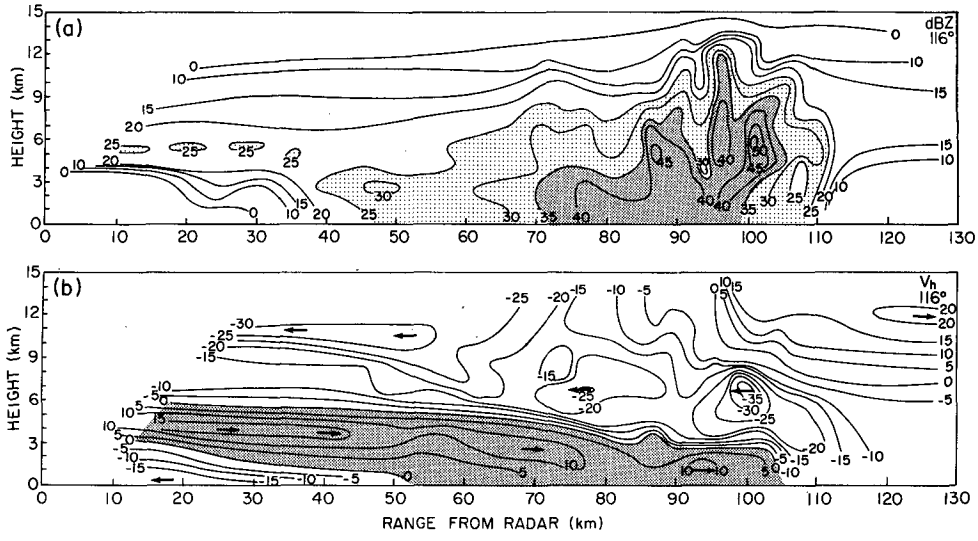

FIG. 12. As in Fig. 11, except for 0701–0713 CST 28 May 1985. Panels (a) and (b) depict reflectivity (dBZ) and system-relative horizontal velocity (m s^{-1}), respectively, along the 116° azimuth direction.

vergence in the stratiform region is consistent with the existence of a mesoscale updraft at mid- to upper-levels and a mesoscale downdraft below, as found in the 22 May 1976 squall line (Ogura and Liou, 1980; Smull and Houze, 1987).

Smull and Houze (1985) noted that the appearance of intense rear inflow coincided with the beginning of the dissipating stage of the 22 May 1976 squall-line system. Horizontal reflectivity maps covering the region traversed by the 10 June PRE-STORM squall line (not shown) indicate that at the time of Figs. 10a and 11, the 10 June system was at a similar stage of evolution. Organized deep convection along the squall line, which had developed at ≈1400 10 June in southwest Kansas, was near its greatest intensity, and later dissipated at ≈0100 11 June in Oklahoma. Thus, rear inflow was fully developed by the 8th hour of the squall line's 11 h lifetime. As in the 1976 case, stratiform cloud and precipitation persisted for several hours following demise of deep convection.

Another detailed example of rear inflow structure is provided by the 28 May 1985 squall line (Fig. 10b). Compared to the 10 June case, the 28 May storm had a narrower stratiform rain region that was most extensive behind the northern end of the line. The squall line propagated toward the east-southeast (i.e., toward the right in the cross section shown in Fig. 12) at about 17 m s^{-1}. In the cross section (Fig. 12b), the leading gust front was marked by strong low-level convergence near 105 km range. Many similarities with respect to the 10 June case are apparent. Rearward velocity perturbations again occurred at midlevels in conjunction with convective cells which fell into an organized multicellular pattern, and the trailing "anvil" echo was much more extensive than that found at mid- to upper-levels ahead of the convection. However, the width of the surface precipitation region reached a maximum of only 70 km on 28 May, as compared to more than 150 km on 10 June. This difference may be related to contrasting rear inflow structure in these two systems. At a distance 50 km behind the gust front, the rear inflow reached a depth of 5 km on 28 May, while at a similar location in the 10 June storm it was confined below 3 km. Increased depth of the rear inflow implies greater potential for evaporation of stratiform precipitation and diminished front-to-rear transport of cloud and precipitation particles into the trailing anvil. The merger of the rear inflow and convective downdraft outflows into a unified current behind the gust front is apparent between 75 and 100 km range in Fig. 12. The increased depth of forward-rushing, evaporatively cooled air behind the gust front (≈3 km on 28 May as compared to <2 km on 10 June) may have contributed to an increased propagation speed (17 m s^{-1} vs 14 m s^{-1}, respectively) as described by previous authors (e.g., Charba, 1974).

In contrast to the 22 May 1976 and 10 June 1985 cases discussed previously, the 28 May storm appeared to be in a relatively steady state near the midpoint of its life cycle. Its convective component, which originated at 1500 on 27 May as a tornadic thunderstorm near the Nebraska/Wyoming border, survived over 12 h after the data shown in Figs. 10b and 12 were taken. It dissipated in northern Mississippi, more than 2000 km distant from its point of initiation. During the period that the squall-line convection was evident (0100 28 May to 1900 28 May), reflectivity data from four Na tional Weather Service radars (Wichita, Kansas; Monnet, Missouri; Little Rock, Arkansas; and Jackson, Mississippi) showed that it maintained its identity. No

discrete "jumps" or reformation of convection ahead of the existing line (of the sort reported by Srivastava et al., 1986) were observed.

4. Comparison with results from the COPT 81 experiment

The 1976 Oklahoma squall line and the two PRE-STORM squall lines previously described all exhibited a strong flow of environmental air across the back edge of their stratiform precipitation regions. Is rear inflow the result of processes occurring within mesoscale convective systems, or does it develop as a consequence of strong midlevel winds in the large-scale environment overtaking and entering these storms? Observations of a West African squall line support the former hypothesis in at least partly accounting for the rear-to-front flow.

In May and June of 1981, several French agencies joined efforts to conduct a coordinated field experiment called COPT 81,[6] which focused on mesoscale convective systems that pass over Upper Volta and Ivory Coast in West Africa. During the early morning hours of 22 June, a fast-moving squall line (propagation speed ≈ 19 m s^{-1}) passed over the COPT 81 network. Analysis of ground-based dual-Doppler radar data for this case has been reported by Chong et al. (1987), and one of their figures is reproduced here as Fig. 13. Figure 13a shows a plan view of the low-level reflectivity pattern (1.5° elevation) for this storm. Major features include a leading line of intense convection bowing forward over the radar site, followed by a transition zone reflectivity minimum and secondary maximum of stratiform precipitation. Wind profiles over the radar were determined from a series of Velocity Azimuth Display (VAD) scans (Browning and Wexler, 1968), and the locations of five such scans are shown by the dashed circles superimposed on the reflectivity pattern in Fig. 13a. Profiles of the system-relative wind normal to the squall line derived from these scans (representative of conditions at the centers of the five circles) are displayed in Fig. 13b. Rear inflow is notably absent in profile 5, which was located closest to the back edge of the stratiform region. However, its shape (i.e., the sense of the vertical shear) bears some similarity to profiles shown for the 22 May 1976 case (cf. Figs. 9b and c). Appreciable front-to-rear flow is indicated above 3 km, as shown in the trailing anvil regions of those cases already discussed. A pronounced minimum of this rearward flow is seen near 2 km. At locations successively closer to the convective line (profiles 4, 3, etc.) this perturbation amplifies and shifts downward, culminating in rear-to-front flow directed from the leading part of the stratiform area into the lower reaches of the convective line (profile 1).

This result strongly indicates that the rear-to-front flow developed in situ in the stratiform region. Roux et al. (1984) and Roux (1985) performed a thermodynamic retrieval from the dual-Doppler observations of the 22 June 1981 squall line, and described the flow entering the convective region as a "density current of cold air generated in the stratiform region . . . resulting from a mesoscale downdraft." They note that this air originated near the 3 km level. This differs from the sructure found in the 22 May 1976 and PRE-STORM cases, where postsquall environmental air crossed the rear edge of the stratiform region in the 3–7 km layer and formed a continuous channel of rear-to-front airflow extending to the squall front. By contrast, the 22 June COPT 81 storm exhibited no rear inflow across the back edge of the stratiform rain area but nonetheless developed rear-to-front flow within the stratiform region. This suggests that the strong rear inflow observed in the Oklahoma and PRE-STORM cases likely developed in response to processes internal to these storms (e.g., microphysical feedbacks) rather than as a direct result of the peculiarities of the winds in the large-scale environments of these storms.

5. Classification of relative airflow at the rear of squall lines with trailing stratiform precipitation

How representative are the four squall lines discussed so far in this paper? Many authors have described aspects of the airflow in and near squall-line systems with areas of trailing stratiform precipitation. We have reviewed the literature and identified a number of studies in which profiles of airflow at the rear of a squall system's rain area were determined quantitatively (Table 1). Note that the table excludes certain papers, such as Newton's important 1950 study, if they described the relative flow at the rear of the mesoscale precipitation area only qualitatively, since from such cases we could not infer the strength of the flow. For each case, we examined the relative wind component normal to the convective line, U_n. As noted in Table 1, some studies were concerned with a single storm while others presented averages or composites for a number of storms. For cases where wind data were available at more than one location, the profile nearest to the rear edge of the stratiform precipitation region was chosen. Examination of the 18 profiles so obtained suggests a natural division of the data into several contrasting flow regimes distinguished by the magnitude of the peak value of relative flow indicated in Table 1.

Profiles for which the peak relative flow [referred to hereafter as $(U_n)_{max}$] was ≥ 5 m s^{-1} are referred to "Rear Inflow" cases. Eight of our 18 profiles fall into this category, which is then subdivided into "Strong Rear Inflow" cases, for which $(U_n)_{max} \geq 10$ m s^{-1} (Fig. 14), and "Weak Rear Inflow" cases, for which $5 \leq (U_n)_{max} < 10$ m s^{-1} (Fig. 15).

[6] *CO*nvection *P*rofonde *T*ropicale 1981.

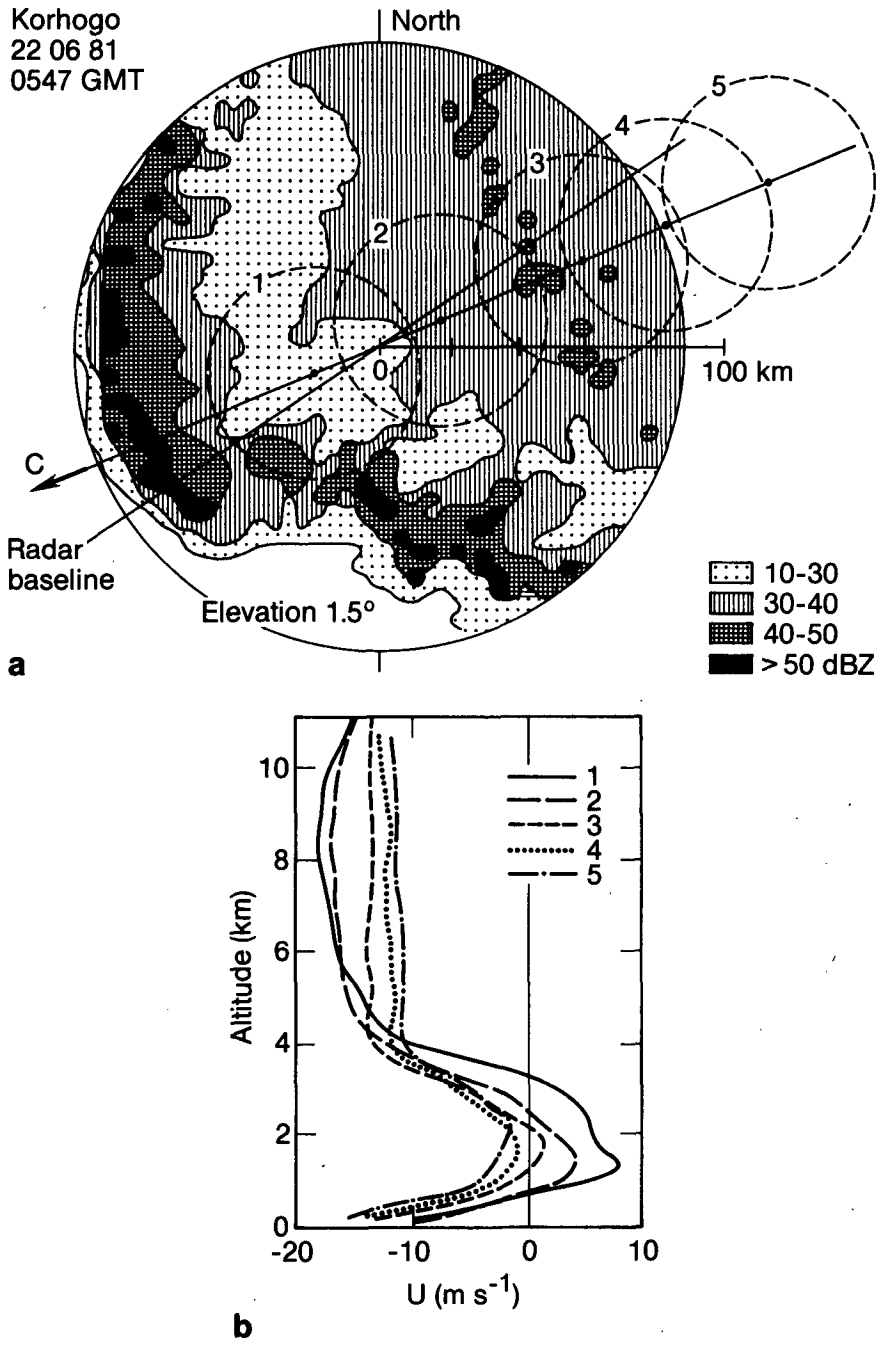

FIG. 13. (a) Low-level (1.5° elevation) reflectivity pattern from the Korhogo radar at 0547 UTC on 22 June 1981. Superimposed circles denote relative locations of conical scans performed in trailing region of the squall line; scans labeled 1–5 were performed at 0529, 0606, 0646, 0709 and 0737 UTC, respectively. (b) Vertical profiles of the system-relative wind component (m s^{-1}) along the squall line's direction of motion (i.e., roughly normal to its mean orientation) derived from conical scans 1–5 described in (a). Positive values denote flow toward the front of the storm (i.e., in the same sense as rear inflow), while negative values denote front-to-rear motion. From Chong et al. (1987).

Three Strong Rear Inflow profiles were obtained (Fig. 14). They are from the Oklahoma and Kansas squall lines discussed in sections 2 and 3. The three profiles are quite similar. Each exhibits a pronounced, jet-like maximum of rear inflow (positive U_n) at middle levels. [Note that the U_n profile in Fig. 9b has been used in Fig. 14 rather than that in Fig. 9c because, even though the latter sounding shows the stronger peak rear inflow (17 m s^{-1}, as indicated in Table 1), it was terminated at a relatively low level thus limiting its comparison with the profiles from the other two Strong Rear Inflow cases represented in Fig. 14.] This kinematic structure

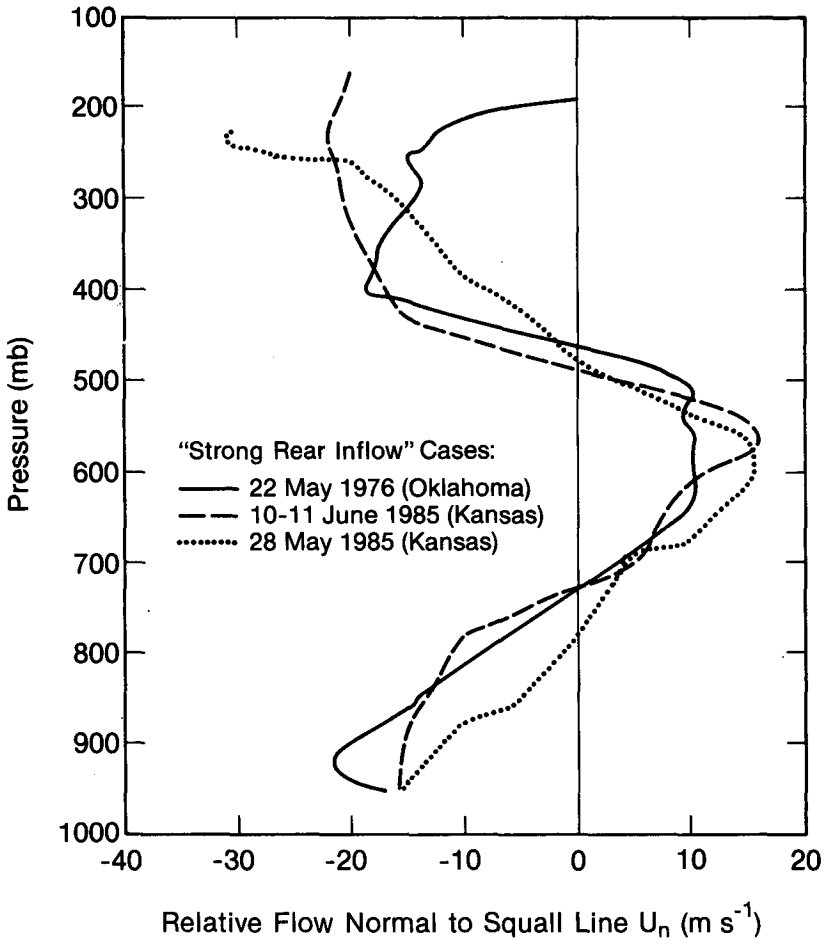

FIG. 14. Vertical profiles of system-relative wind component normal to the convective line (U_n, m s^{-1}) behind squall line systems with trailing stratiform precipitation for "Strong Rear Inflow" cases (described in text).

is associated with the influx of dry midlevel environmental air across the rear boundary of the stratiform region. Additionally, quite strong front-to-rear relative flow is indicated both above and below the rear inflow in each of these cases. That above corresponds to the trailing cloud layer from which stratiform rain falls, while that below is decidedly subsaturated and originates as a thin surface layer in the convective region that progressively deepens as it crosses the stratiform region (see Figs. 11 and 12). The mean of the three profiles in Fig. 14 is shown in Fig. 17. The jet-like rear inflow is maximum near 550 mb. If the sounding in Fig. 9c had been used to represent the 22 May 1976 storm instead of the one from Fig. 9b, the peak would have been at a somewhat lower altitude, but the basic character of the mean curve would not be altered. Of course, three cases is a limited sample on which to base a mean curve; however, the high degree of similarity of the profiles in these three independent cases gives some confidence that they represent a recurrent type of storm structure.

In contrast to the similarity of the three Strong Rear Inflow profiles, the five Weak Rear Inflow profiles are widely varying, especially at middle to upper levels (Fig. 15). Despite this variability, similarities to the Strong Rear Inflow profiles can be seen if the curves are examined individually:

- Zipser and Matejka (1982): This curve represents a midlatitude squall line observed in Illinois. Its shape strongly resembles that of the Strong Rear Inflow profiles in Fig. 14.
- Houze (1977): This profile obtained at the rear of a tropical oceanic squall system is also quite similar to the Strong Rear Inflow cases except that the layer of positive velocities is interrupted by a speed minimum near its center, just below 600 mb. While this aberration may be due to measurement errors common to the GATE rawinsonde data [e.g., see the U.S. GATE[7]

[7] Global Atmospheric Research Program Atlantic Tropical Experiment.

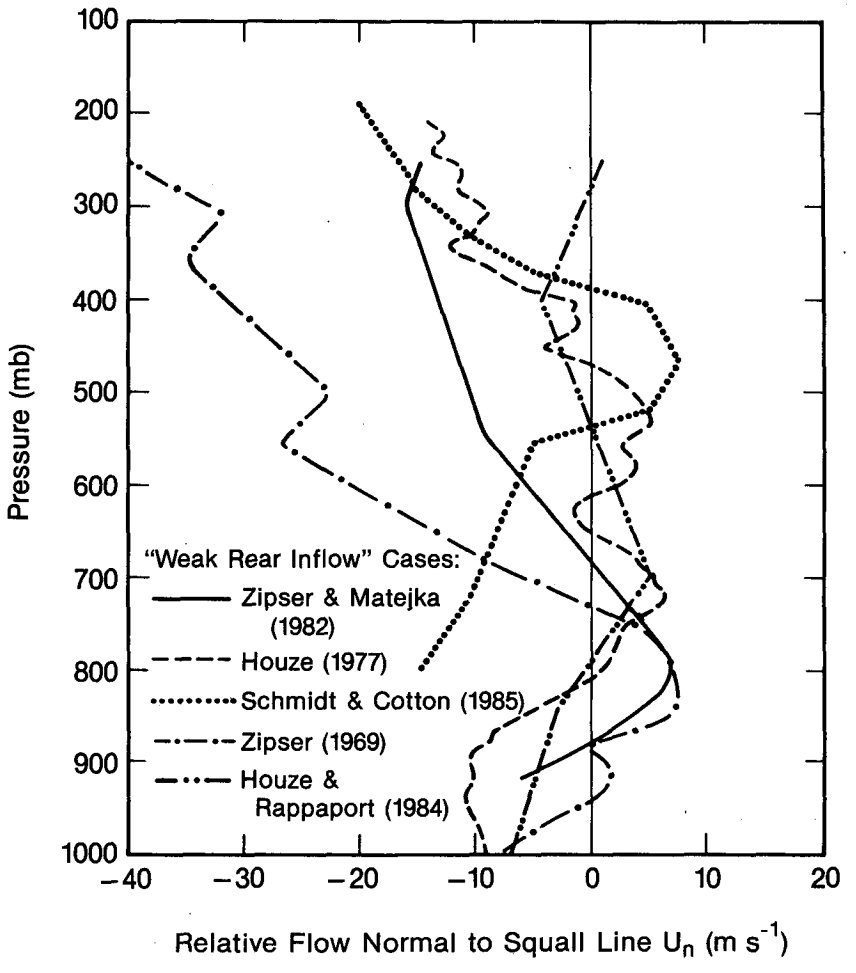

FIG. 15. As in Fig. 14, except for Weak Rear Inflow cases.

Workshop Report (1977)], it is supported by several other soundings (not shown).

• Schmidt and Cotton (1985): This case, which occurred in eastern Montana, exhibited a sharp jet of rear inflow lying between layers of strong shear above and below the jet core much as in the Strong Rear Inflow profiles. However, the maximum inflow jet appeared at a much higher level than was observed in the Strong Rear Inflow cases. The upward shift of the entire flow profile in this case may have been partly due to the elevated terrain height, which was near 1 km MSL. By comparison, most of the cases in Fig. 14 occurred over terrain at about 0.3 km MSL.

• Zipser (1969): This tropical oceanic system exhibited the basic character of the storms in the Strong Rear Inflow group. However, its strongest inflow occurred at a much lower level (800 mb) than seen in the mean Strong Rear Inflow profile (550 mb). Consequently, the front-to-rear flow at higher levels extended through a much deeper layer (700 mb to the tropopause) than in the Strong Rear Inflow cases. This peculiar structure may have derived from the large-scale environment in the tropical south Pacific, where the storm propagated westward in the face of strong upper-level westerlies.

• Houze and Rappaport (1984): This tropical case also exhibited a rear inflow peak at an altitude somewhat below that of the mean Strong Rear Inflow profile. It was also characterized by a weaker than usual front-to-rear flow aloft. It could be reasonably argued that this profile resembles more closely the Stagnation Zone cases to be described than the Strong Rear Inflow cases.

Ten of the eighteen U_n profiles we examined were characterized by very weak or nonexistent rear inflow [$(U_n)_{max} < 5$ m s^{-1}]. This group of profiles, designated as "Stagnation Zone cases," is shown in Fig. 16. These storms [or in the case of Obasi (1974) and Betts et al. (1976), composites of several storms] exhibit appreciable front-to-rear relative airflow in the lower and upper troposphere, as do the Weak and Strong Rear Inflow cases. However, in place of strong rear inflow they exhibit a 200–300 mb (≈2–3 km) deep layer of air moving roughly at the speed of the system. This kinematic

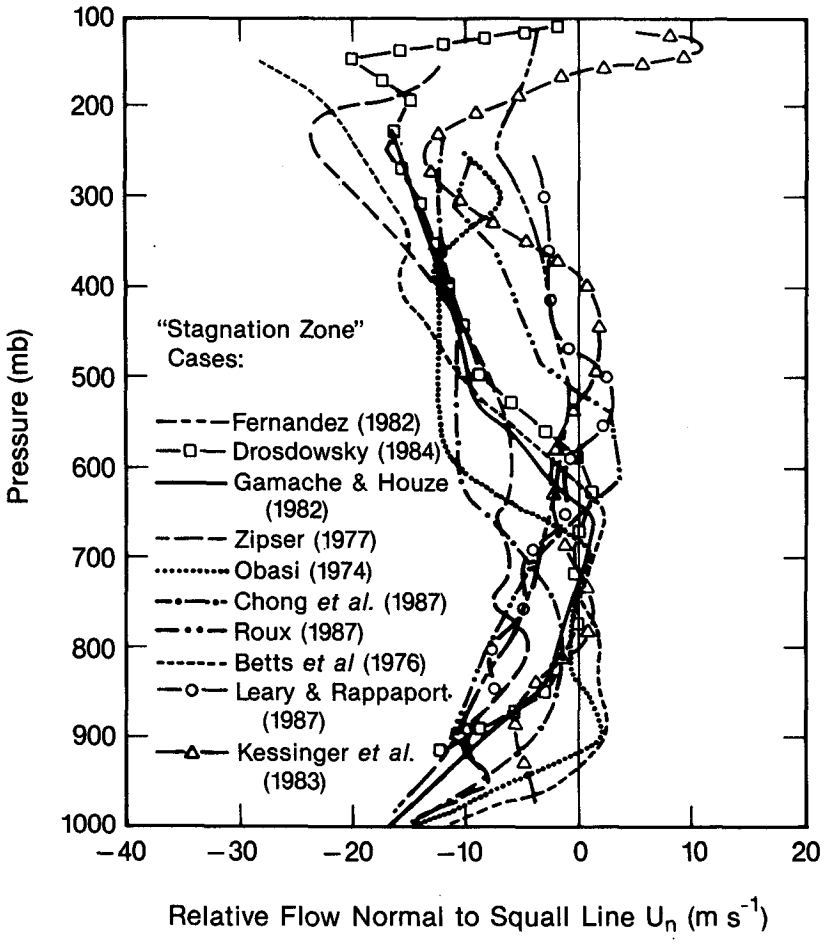

FIG. 16. As in Fig. 14, except for Stagnation Zone cases. Leary and Rappaport (1987) curve corresponds to the 1900 8 June sounding, used in part to construct their Fig. 33; detailed wind data were obtained directly from the authors.

structure lends itself to the notion of a stagnation zone (in the relative flow) at midlevels near the back edge of these storms. This sample is dominated by tropical squall lines, but includes storms from diverse regions [to wit, Fig. 16 includes profiles for storms over the eastern tropical Atlantic (Gamache and Houze, 1982), the Carribean (Zipser, 1977), equatorial West Africa (Obasi, 1974; Fernandez, 1982; Chong et al., 1987; Roux, 1987), Venezuela (Betts et al., 1976), Northern Australia (Drosdowsky, 1984), West Texas (Leary and Rappaport, 1987) and Oklahoma (Kessinger et al., 1983)].

Of the Stagnation Zone cases in Fig. 16, the profile which failed most strongly to exhibit midlevel rear inflow at the back edge of the system was that of Zipser (1977). It is possible that the rawinsonde sampling was inadequate to describe fully the relative flow at the rear of this system. Aircraft measurements documented a limited region of weak rear-to-front flow near 800 mb at a distance $\approx$ 50 km behind the squall front [see Fig. 3 of Zipser (1977)], perhaps analogous to the pattern shown by Chong et al. (1987, see our Fig. 13). The Leary and Rappaport (1987) Stagnation Zone case also exhibited rear-to-front flow in a limited region within the stratiform region; moreover, this rear-to-front flow was associated with a mesoscale vortex in the stratiform precipitation region. The descriptions of these three Stagnation Zone cases suggest that processes internal to the squall system can generate rear-to-front flow within the system itself, but further indicate that this frontward flow need not extend across the back edge of the mesoscale rain area as in the Strong Rear Inflow cases.

The mean of the Stagnation Zone profiles is shown in Fig. 17, where it is compared with the mean of the Strong Rear Inflow profiles. The Stagnation Zone profile differs markedly from the Strong Rear Inflow profile. The latter exhibits stronger front-to-rear flow at lower and upper levels than does the Stagnation Zone profile. The maximum U_n of the Strong Rear Inflow profile is not only greater in magnitude (+14 m s^{-1} compared to −2 m s^{-1} in the mean Stagnation Zone

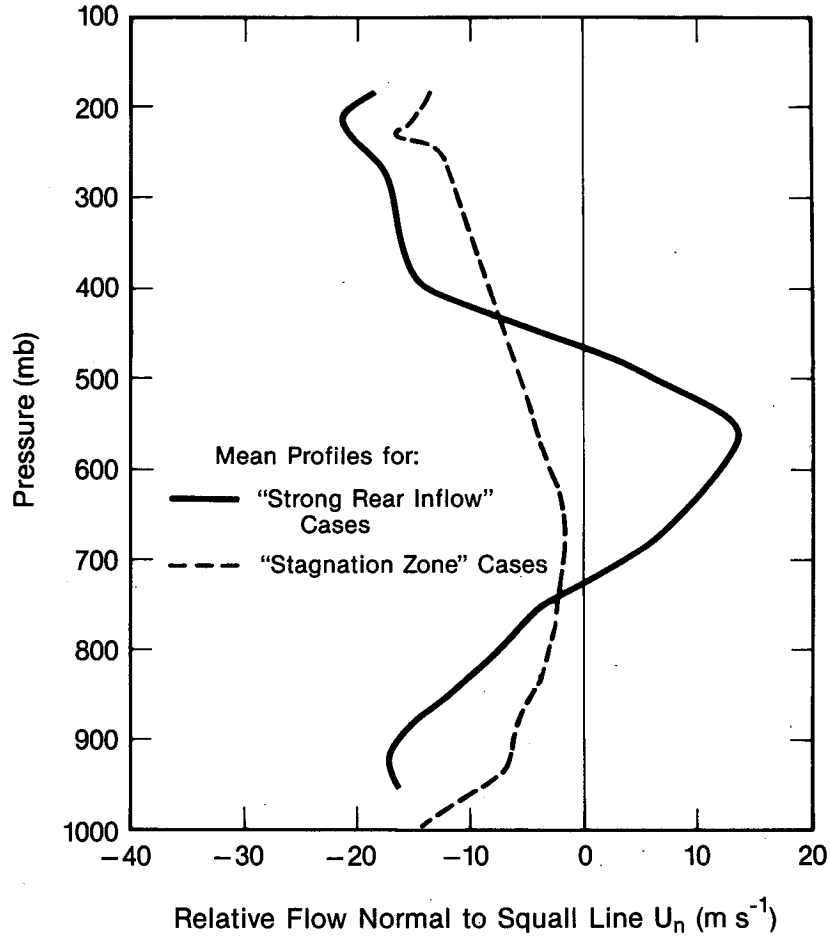

FIG. 17. Mean profiles of system-relative wind component normal to the convective line (U_n, m s^{-1}) for Strong Rear Inflow cases (solid curve) and Stagnation Zone cases (dashed curve) shown in Figs. 14 and 16, respectively.

profile), but located at a much greater altitude (550 mb compared to 650–750 mb). These differences suggest that the Strong Rear Inflow and Stagnation Zone are distinct modes of airflow in squall lines with trailing stratiform precipitation areas.

Some of the differences between the Strong Rear Inflow and Stagnation Zone cases may be due to storm evolution. For example, it is conceivable that, if sampled in its formative stage, a Rear Inflow case might be mistakenly interpreted as belonging in the Stagnation Zone group. Also, limited spatial coverage by soundings in some cases might not fully resolve the rear-inflow jet even though it was present. However, Fig. 16 includes profiles for two cases in which the Stagnation Zone was evident in the mature to dissipating stages of storms with extensive sounding coverage (Gamache and Houze, 1982; Leary and Rappaport, 1987). These results further indicate that the Stagnation Zone is a separate mode of airflow.

No tendency for storms in the Rear Inflow category to propagate faster (relative to the ground) than those in the Stagnation Zone group is suggested by the propagation speeds shown in Table 1. Barnes and Sieckman (1984) considered the mean properties of three "fast-moving" tropical squall lines. Two of these three cases have been included among the profiles in our survey [viz., the cases studied by Gamache and Houze (1982) and Houze and Rappaport (1984)]. The Gamache-Houze case was included in our Stagnation Zone group (Fig. 16), while the Houze-Rappaport case fell into the Weak Rear Inflow category (Fig. 15). It is therefore not surprising that the relative flow in the wake of Barnes and Sieckman's "fast-moving" tropical squall lines is weaker than that seen in our Strong Rear Inflow profiles. (Wake profiles were described but not expressly shown by Barnes and Sieckman.) Apparently, our Strong Rear Inflow, Wear Rear Inflow and Stagnation Zone designations represent different modes of Barnes and Sieckman's fast-moving prototype. Their "slow-moving" cases do not appear to correspond to the types of cases that we have considered (i.e., squall lines with trailing stratiform precipitation regions).

6. Conclusions

Examination of NSSL and PRE-STORM data from three Kansas and Oklahoma squall lines trailed by stratiform precipitation, together with an inclusive review of the literature concerning airflow in this type of storm, has revealed rather distinct regimes of system-relative flow behind these systems. In all cases, the relative flow normal to the line tended to be front-to-rear at both upper and lower levels, with the front-to-rear flow decreasing at midlevels. In some storms, referred to as Rear Inflow cases, the sign of the relative flow in this midlevel minimum reversed, so that air flowed into the storm across the back edge. In Strong Rear Inflow cases, in which the flow across the back edge of the storm was ≥ 10 m s^{-1}, the inflow was jet-like, with peak magnitudes of ≈ 13 m s^{-1} centered near the 550 mb level. Weak Rear Inflow cases (5–10 m s^{-1} peak values of inflow) exhibited relative flow profiles with a variety of structures; the rear inflow maximum was sometimes located at much higher altitudes than in the Strong Rear Inflow cases and sometimes considerably lower. A third category of storms, termed Stagnation Zone cases, showed little if any rear inflow; instead, midlevel air near their back edges moved roughly at the speed of these systems. Over half of the studies referred to were described as Stagnation Zone cases. The mean relative flow profile for these cases differed markedly from that of the Strong Rear Inflow cases. Instead of the strong jet-like maximum near 550 mb, the profile was characterized by a broader maximum in which the maximum relative flow was ≈ -2 m s^{-1} and located at much lower levels (between 650 and 750 mb). In addition, the front-to-rear flow above and below the relative flow was weaker in the Stagnation Zone profile than in the Strong Rear Inflow profile. Observations of Stagnation Zone flow in the mature and late stages of storms support its interpretation as a distinct mode of airflow organization for squall lines with trailing stratiform regions rather than merely being an early stage preceding the realization of strong rear inflow. The Stagnation Zone cases were dominated by, but not restricted to, tropical squall lines, while the three Strong Rear Inflow cases were midlatitude storms from Kansas and Oklahoma. The Weak Rear Inflow cases included a mix of tropical and midlatitude squall lines.

The NSSL and PRE-STORM data supplemented the previously published studies of squall lines with trailing stratiform regions by providing detailed views of three Strong Rear Inflow cases. Sounding data from the NSSL case demonstrate the association of strong rear inflow with depressed values of θ_w, and show that the axis of strongest rear inflow slopes downward toward the front of these storms. As the rear inflow air passes through the melting level, its θ_w is lowered at the rate of a few degrees Celsius per hour. Doppler radar data from the PRE-STORM cases show that the rear inflow jet extends across the system as an uninterrupted channel of rear-to-front velocities stretching downward from mid- to upper levels at the back edge of the stratiform rain area toward the lower reaches of the convective region. There, the rear inflow air combines with outflow from convective-cell downdrafts to bolster flow behind the leading gust front and thus constitutes an important feedback of the mesoscale circulation upon the parent squall-line convection. Comparison of the two PRE-STORM systems further suggests that increased depth of the rear inflow (and accompanying decreases in depth of the cloud- and precipitation-laden layer of front-to-rear flow above) may contribute to a decrease in the width of the stratiform region.

Our examination of the NSSL and PRE-STORM cases has identified several features in addition to rear inflow that are common to these storms. These include organized multicellular structure of the deep convection (similar to that described by Browning et al., 1976), limited extent of the leading anvil, a well defined bright band echo associated with melting precipitation in the trailing stratiform region, separation of the convective and trailing stratiform regions by a "transition zone" of decreased radar reflectivity at low levels, and a prominent maximum of system-relative, front-to-rear flow, which traverses these storms at mid- to upper-levels and is enhanced in the vicinity of convective cells. The convergence of the rear inflow with this opposing front-to-rear flow is almost certainly a factor in forcing the mesoscale updraft/downdraft circulation in the stratiform rain area [which was documented in the 22 May 1976 case by Ogura and Liou (1980)].

Front-to-rear flow at upper levels is also observed in Stagnation Zone cases, and midlevel convergence is implied in those cases by the zone of stagnation lying adjacent to upward sloping rearward relative flow. As in the Rear Inflow cases, this convergence may be linked to mesoscale ascent and descent in their trailing regions (e.g., Gamache and Houze, 1982; Chong et al., 1987).

Data from several of the Stagnation Zone cases have provided special insight into the airflow structure internal to squall systems with trailing stratiform precipitation. While (by definition) no appreciable rear inflow occurred at the back edge of these storms, rear-to-front flow was observed to develop at midlevels in the interior of their stratiform regions. This behavior was suggested by the aircraft data obtained 50 km behind the squall line studied by Zipser (1977, see our section 5) and has been more extensively documented the stagnation zone cases studied by Chong et al. (1987, see our section 4) and Leary and Rappaport (1987). Chong et al. found that the rear-to-front flow in the interior of the stratiform region extended forward and downward into the leading convective region. Leary and Rappaport found a similar slope and further showed the forward-flowing current to be intimately related to a midlevel cyclonic

circulation centered on the stratiform region. From these studies, it appears that physical processes internal to the mesoscale system are capable of generating rear-to-front flow behind the convective line without the aid of ambient flow entering the storm.

On the basis of observations described in this paper, we may speculate on the mechanisms responsible for the development of rear inflow. For this purpose, it is convenient to refer to the conceptual model (Fig. 1). It is important to note that at this apparently early stage in the rear inflow's development, rear-to-front relative airflow was found not only at the extreme rear of the stratiform region (near −115 km in Fig. 1), but also at low levels across the transition zone and convective regions (between −50 and +15 km). This suggests that two separate mechanisms may have acted to establish a continuous current of rear inflow across the storm like that in the two PRE-STORM cases (Figs. 11 and 12).

Although they did not explicitly address pressure gradient effects (which were undoubtedly quite important), Smull and Houze (1987) used results of a dual-Doppler radar analysis to estimate accelerations due to vertical flux of horizontal momentum in the convective region of the 22 May storm. The net effect of these transports was to accelerate air below 3 km toward the front of the storm, while parcels in the 3–9 km layer were accelerated rearward (with the strongest accelerations diagnosed near the level where convective-scale speed maxima were superimposed on the midlevel rearward flow in Fig. 1). Similar accelerations were diagnosed by LeMone (1983) and LeMone et al. (1984) from profiles of vertical momentum flux in tropical cumulonimbus lines. They found these accelerations to be closely related to a hydrostatically induced perturbation pressure minimum that developed immediately under (and thus behind) warm convective updrafts, which sloped rearward with height. The existence of an analogous feature in midlatitude squall lines awaits the diagnosis of their thermodynamic and perturbation pressure fields from Doppler radar observations.

At the same time as these accelerations were occurring in the lower reaches of the convective region, rear inflow was just breaching the back edge of the stratiform echo at midlevels (nearly 100 km distant). The absence of strong vertical transports in that part of the storm and its remoteness suggests that this feature was due to different processes. In a numerical study of mesoscale motions accompanying parameterized convection, Brown (1979) found the development of a pronounced midlevel mesolow in a region of stratiform precipitation. This geopotential depression is attributable to the combined effects of latent heat release aloft (accompanying mesoscale saturated ascent and freezing of supercooled water in the trailing "anvil" cloud) and evaporative cooling below (as stratiform precipitation falls through markedly subsaturated air). [The latter is enhanced by cooling due to melting, as shown by Leary and Houze (1979), and as indicated by our examination of the 22 May 1976 NSSL case (section 2 of this paper).] Hydrostatic adjustment to this vertically displaced heat source and sink results in increased thickness aloft, decreased thickness in the lower troposphere, and thus engenders lower geopotential heights in the midtroposphere. The resulting horizontal pressure gradient force would be expected to draw air into the storm at middle levels. While details of the evolution and placement of such a mesolow within the trailing stratiform region remain unclear, it seems plausible that such a feature may act in conjunction with the aforementioned processes in the convective region to establish the uninterrupted conduit of rear-to-front flow seen in the Rear Inflow cases. Although substantial questions remain unanswered, the observations presented here represent a major step toward understanding the structure and mechanism of rear inflow and other commonly observed features of mesoscale convective systems.

Acknowledgments. We especially thank E. Kessler and P. Ray for their assistance with the NSSL data analysis and the NCAR Field Observing Facility staff for their expert collection of the PRE-STORM data Dean Churchill provided sounding analysis software. Comments and suggestions made by the reviewers and J. Brown substantially improved the paper. This research was supported by the National Science Foundation under Grants ATM8419543 and ATM8413546, the National Oceanic and Atmospheric Administration, the National Severe Storms Laboratory under Grant NA80RAD00025, and the National Center for Atmospheric Research.

APPENDIX

Determination of Horizontal Velocities Analyzed in Vertical Cross Sections

System-relative horizontal velocities (V_h) have been derived from the observed radial velocities (V_r) using the relation

$$V_h = V_r/\cos\alpha + V_t \tan\alpha - V_s \qquad \text{(A1)}$$

where α is the elevation angle, V_t is the terminal fallspeed (positive downward), and V_s is the component of the system's motion along the direction of the cross section (positive away from the radar). For consistency, V_r and V_h are also taken positive away from the radar. In writing Eq. A1, the radial component of vertical air motion (w), which is negligible in the absence of convective drafts at close range, has been neglected. The V_t was estimated from the reflectivity factor Z using separate relations for solid and liquid precipitation:

$$V_t = 0.817Z^{0.063} \quad \text{for snow} \qquad \text{(A2)}$$

$$V_t = 2.6Z^{0.107} \quad \text{for rain.} \qquad \text{(A3)}$$

Fallspeeds given by Eq. (A2) were assumed at heights above 5 km, while below 4 km Eq. (A3) was applied.

In the layer between 4 and 5 km, a linear combination of these two results was used. The first relationship (A2) was derived by Atlas et al. (1973) for snow, while the second is taken from Joss and Waldvogel (1970) and is for rain. Since these relationships are valid at ground level, a density–height correction factor suggested by Foote and du Toit (1969) was employed to render them applicable at other altitudes. Specifically, the right-hand side of (A2) and (A3) was multiplied by the density–height correction factor $[\rho_0/\rho(z)]^{0.4}$, where $\rho(z) = \rho_0 \exp(-z/9.2)$ and z is height (in kilometers) above reference level z_0. The scale height (9.2 km) was determined from a sounding taken at Hinton, Oklahoma (HNT) at 1430 on 22 May 1976. As this technique of computing horizontal velocity is sensitive to errors in the assumed fallspeed at large elevation angles, the analysis was limited to regions where $\alpha < 20°$.

Finally, data points were shifted horizontally to correct for the effects of system translation during the time interval required to complete a volume scan ($\approx$10 min). This correction resulted in a maximum displacement of about 5 km for the highest elevation angles, but was negligible throughout most of the cross sections.

REFERENCES

Atlas, D., R. C. Srivastava and R. S. Sekhon, 1973: Doppler radar characteristics of precipitation at vertical incidence. *Rev. Geophys. Space Phys.*, **11**, 1–35.

Augustine, J. A., and E. J. Zipser, 1987: The use of wind profilers in a mesoscale experiment. *Bull. Amer. Meteor. Soc.*, **68**, 4–17.

Barnes, G. M., and K. Sieckman, 1984: The environment of fast- and slow-moving tropical mesoscale convective cloud lines. *Mon. Wea. Rev.*, **112**, 1782–1794.

Betts, A. K., R. W. Grover and M. W. Moncrieff, 1976: Structure and motion of tropical squall lines over Venezuela. *Quart. J. Roy. Meteor. Soc.*, **102**, 395–404.

Brown, J. M., 1979: Mesoscale unsaturated downdrafts driven by rainfall evaporation: A numerical study. *J. Atmos. Sci.*, **36**, 313–338.

Browning, K. A., and R. Wexler, 1968: The determination of kinematic properties of a wind field using Doppler radar. *J. Appl. Meteor.*, **7**, 105–113.

——, J. C. Fankhauser, J. P. Chalon, P. J. Eccles, R. C. Strauch, F. H. Merrem, D. J. Musil, E. L. May and W. R. Sand, 1976: Structure of an evolving hailstorm. Part V: Synthesis and implications for hail growth and hail suppression. *Mon. Wea. Rev.*, **104**, 603–610.

Charba, J. B., 1974: Application of gravity current model of analysis of squall-line gust fronts. *Mon. Wea. Rev.*, **102**, 140–156.

Chong, M., P. Amayenc, G. Scialom and J. Testud, 1987: A tropical squall line observed during the COPT 81 experiment in West Africa. Part I: Kinematic structure inferred from dual-Doppler radar data. *Mon. Wea. Rev.*, **115**, 670–694.

Cunning, J. B., 1987: The Oklahoma-Kansas preliminary regional experiment for STORM-Central. *Bull. Amer. Meteor. Soc.*, **67**, 1478–1486.

Davies-Jones, R. P., 1974: Discussion of measurements inside high-speed thunderstorm updrafts. *J. Appl. Meteor.*, **13**, 710–717.

Drosdowsky, W., 1984: Structure of a northern Australian squall line system. *Aust. Meteor. Mag.*, **32**, 177–183.

Fernandez, W., 1982: Environmental conditions and structure of the west African and eastern tropical Atlantic squall lines. *Arch. Meteor. Geophys. Bioklim.*, **A31**, 71–89.

Foote, G. B., and P. S. du Toit, 1969: Terminal velocity of raindrops aloft. *J. Appl. Meteor.*, **8**, 249–253.

Gamache, J. F., and R. A. Houze, Jr., 1982: Mesoscale air motions associated with a tropical squall line. *Mon. Wea. Rev.*, **110**, 118–135.

Houze, R. A., Jr., 1977: Structure and dynamics of a tropical squall-line system. *Mon. Wea. Rev.*, **105**, 1540–1567.

——, and P. V. Hobbs, 1982: Organization and structure of precipitating cloud systems. *Adv. Geophys.*, **24**, Academic Press, 225–315.

——, and E. N. Rappaport, 1987: The life cycle and internal structure of a mesoscale convective complex. *Mon. Wea. Rev.*, **115**, 1503–1527.

Joss, J., and A. Waldvogel, 1970: Raindrop size distribution and Doppler velocities. *Preprints 14th Conf. on Radar Meteorology*, Tucson, Amer. Meteor. Soc., 153–156.

Kessinger, C. J., P. S. Ray and C. E. Hane, 1983: An Oklahoma squall line: A multiscale observational and numerical study. *CIMMS Report No. 34*, Cooperative Institute for Mesoscale Meteorological Studies, 211 pp.

Leary, C. A., and R. A. Houze, Jr., 1979: Melting and evaporation of hydrometeors in precipitation from the anvil clouds of deep tropical convection. *J. Atmos. Sci.*, **36**, 669–679.

——, and E. N. Rappaport, 1987: The life cycle and internal structure of a mesoscale convective complex. *Mon. Wea. Rev.*, **115**, 1503–1527.

LeMone, M. A., 1983: Momentum transport by a line of cumulonimbus. *J. Atmos. Sci.*, **40**, 1815–1834.

——, G. M. Barnes and E. J. Zipser, 1984: Momentum flux by lines of cumulonimbus over the tropical oceans. *J. Atmos. Sci.*, **41**, 1914–1932.

Newton, C. W., 1950: Structure and mechanisms of the prefrontal squall line. *J. Meteor.*, **7**, 210–222.

Obasi, G. O. P., 1974: The environmental structure of the atmosphere near West African disturbance lines. *Preprints Int. Tropical Meteorology Meeting*, Nairobi, Amer. Meteor. Soc., 62–66.

Ogura, Y., and M. T. Liou, 1980: The structure of a midlatitude squall line: A case study. *J. Atmos. Sci.*, **37**, 553–567.

Roux, F., 1985: Retrieval of thermodynamic fields from multiple-Doppler radar data using the equations of motion and the thermodynamic equation. *Mon. Wea. Rev.*, **113**, 2142–2157.

——, 1987: Les lignes de Grains de COPT 81: Environnement, precipitations, cinematique et thermodynamique. Ph.D. thesis, University of Paris, 368 pp.

——, J. Testud, M. Payen and B. Pinty, 1984: West African squall line thermodynamic structure retrieved from dual-Doppler radar observations. *J. Atmos. Sci.*, **41**, 3104–3121.

Schmidt, J. M., and W. R. Cotton, 1985: Bow echo structure and evolution within a high plains mesoscale squall line. *Preprints 14th Conf. on Severe Local Storms*, Indianapolis, Amer. Meteor. Soc., 77–80.

Smull, B. F., and R. A. Houze, Jr., 1985: A midlatitude squall line with a trailing region of stratiform rain: Radar and satellite observations. *Mon. Wea. Rev.*, **113**, 117–133.

——, and ——, 1987: Dual-Doppler radar analysis of a midlatitude squall line with a trailing region of stratiform rain. *J. Atmos. Sci.*, **44**, 2128–2148.

Srivastava, R. C., T. J. Matejka and T. J. Lorello, 1986: Doppler radar study of the trailing anvil region associated with a squall line. *J. Atmos. Sci.*, **43**, 356–377.

U.S. GATE Central Program Workshop Report, 1977: National Center for Atmospheric Research, P.O. Box 3000, Boulder, CO 80307, 723 pp.

Zipser, E. J., 1969: The role of organized unsaturated convective downdrafts in the structure and rapid decay of an equatorial disturbance. *J. Appl. Meteor.*, **8**, 799–814.

——, 1977: Mesoscale and convective-scale downdrafts as distinct components of squall-line circulation. *Mon. Wea. Rev.*, **105**, 1568–1589.

——, and T. J. Matejka, 1982: Comparison of radar and wind cross-sections through a tropical and a midwestern squall line. *Preprints 12th Conf. on Severe Local Storms*, San Antonio, Amer. Meteor. Soc., 342–345.